

# Calculation of multiplet structures of $\text{Cr}^{3+}$ and $\text{V}^{3+}$ in $\alpha\text{-Al}_2\text{O}_3$ based on a hybrid method of density-functional theory and the configuration interaction

Kazuyoshi Ogasawara and Takugo Ishii

*Department of Materials Science and Engineering, Kyoto University, Sakyo-ku, Kyoto 606-8501, Japan*

Isao Tanaka

*Department of Energy Science and Technology, Kyoto University, Sakyo-ku, Kyoto 606-8501, Japan*

Hirohiko Adachi

*Department of Materials Science and Engineering, Kyoto University, Sakyo-ku, Kyoto 606-8501, Japan*

(Received 2 November 1998; revised manuscript received 27 July 1999)

The multiplet structures of  $\text{Cr}^{3+}$  and  $\text{V}^{3+}$  in  $\alpha\text{-Al}_2\text{O}_3$  ( $\alpha\text{-Al}_2\text{O}_3:\text{Cr}^{3+}$  and  $\alpha\text{-Al}_2\text{O}_3:\text{V}^{3+}$ ) have been calculated based on a hybrid method of the density-functional theory (DFT) and the configuration interaction (CI) calculation (DFT-CI approach). The correction to the electron correlation effects was estimated from the consistency between the single-electron DFT calculation and the many-electron DFT-CI calculation. The observed multiplet structures were predicted satisfactorily without referring to any experimental data. Using the explicitly obtained many-electron wave functions, the intensities of the electric-dipole transition were also calculated numerically and the polarization of the absorption spectra of  $\alpha\text{-Al}_2\text{O}_3:\text{Cr}^{3+}$  (ruby) was qualitatively reproduced.

## I. INTRODUCTION

As is well known, the ligand-field theory has been successful in explaining the optical properties of transition-metal (TM) ions in crystals.<sup>1</sup> The multiplets of the TM ions in the octahedral (or tetrahedral) symmetry are expressed in terms of the Racah parameters ( $B$  and  $C$ ) and the crystal-field parameter ( $\Delta$ ). However, these parameters are determined from the optical spectra under a certain trial assignment of the observed peaks. Therefore the correct parameters cannot be obtained unless the optical spectrum of the material is available and well understood. Even if the correct parameters are determined from the experimental data, the meanings of the parameters are somewhat ambiguous, since the effect of covalency and the effect of electron correlations are absorbed in the empirical parameters during the fitting process, although this was one of the essential reasons for the great success of the ligand-field theory as an “empirical” method. Moreover, the traditional analysis cannot provide the explicit form of the many-electron wave functions. Therefore the transition probability between the multiplets cannot be estimated without a drastic approximation such as the closure.<sup>1</sup>

In order to circumvent the above-mentioned shortcomings of the traditional approach, a first-principles calculation is quite necessary. In the present paper, we have calculated the multiplet structures of ruby ( $\alpha\text{-Al}_2\text{O}_3:\text{Cr}^{3+}$ ) and  $\alpha\text{-Al}_2\text{O}_3:\text{V}^{3+}$  based on a hybrid method of the density-functional theory (DFT) and the configuration interaction (CI) calculation. Ruby is, needless to say, a beautiful gemstone and known as the first solid-state laser in history.<sup>2</sup> The so-called ruby pressure scale using its fluorescence lines is particularly popular in high-pressure science<sup>3–5</sup> because of the simplicity and the accuracy of optical measurements in the diamond-anvil cell (DAC) experiments. The electronic structure of ruby has been studied extensively based on the

ligand-field theory with some additional parameters such as the trigonal-field parameter or the spin-orbit interaction parameter.<sup>6–9</sup> However, the reports on the first-principles calculation of the multiplet structure of ruby are rather limited.<sup>10–12</sup> The electronic structure of  $\alpha\text{-Al}_2\text{O}_3:\text{V}^{3+}$  has also been studied in detail based on a similar semiempirical approach.<sup>13,14</sup>

Based on the single-electron cluster calculation, theoretical prediction of the optical spectra of ruby has been attempted by Ohnishi and Sugano<sup>10</sup> and Xia *et al.*<sup>11</sup> using analytic relations between the molecular-orbital energies and the multiplet energies. However, in these works, only the positions of the  $R$  line ( ${}^2E$ ) and the  $U$  band ( ${}^4T_2$ ) were estimated, since simple relations could not be obtained for other multiplets.

Recently, a first-principles calculation of the entire multiplet structure of ruby has been carried out by Duan *et al.*<sup>12</sup> and the pressure dependence of the multiplet structure of ruby has been well reproduced. They predicted an anomalous local relaxation which could explain the observed frequency shifts. However, their calculation was based on the analytic multiplet approach using the atomic Racah parameters and the matrix elements were calculated in the octahedral approximation. Although the effect of the covalency was taken into account by multiplying the orbital deformation parameters on the electron-electron repulsion integrals, these parameters were adjusted to the optical spectra of ruby under zero pressure for the quantitative analysis of the pressure dependence of the multiplet structure. Moreover, it would be difficult for their approach to predict the intensity of the optical spectra, since the optical spectra of ruby are dominated by the electric-dipole transitions arising from the trigonal distortion of the many-electron wave functions which was ignored in their calculation.

Recently, we have also calculated the multiplet structure

of ruby<sup>15</sup> based on a computational approach similar to that proposed by Watanabe and Kamimura,<sup>16,17</sup> which was a hybrid method of the spin-restricted density-functional theory (SRDFT) and the configuration interaction (CI) calculation (SRDFT-CI approach). In this calculation, the effect of covalency was directly taken into account through the numerical calculation of the electron-electron repulsion integrals using the molecular orbitals obtained by the cluster calculation. However, there are two shortcomings in our previous approach. One is the computational method of the matrix elements of the many-electron Hamiltonian and the other is the effect of electron correlations.

The many-electron Hamiltonian for the impurity electrons ( $H$ ) consists of the effective single-electron Hamiltonian including the potential from the core and valence electrons ( $h$ ) and the electron-electron repulsion interaction among the impurity electrons. For the calculation of the matrix elements of  $H$ , the explicit form of  $h$  should be known. However, the actual calculation of the exchange-correlation part of  $h$  is somewhat complicated. Therefore, in our previous calculation, we adopted a more efficient method proposed by Fazio, Caldas, and Zunger (FCZ approach). In this method, all single-electron mean-field effects are formally separated from the many-electron effects.<sup>18,19</sup> As a result, the matrix elements of  $h$  can be obtained without knowing the explicit form of  $h$ . Although the average energy of each state in the  $O_h$  notation could be reproduced well by this approach, the trigonal splits of these states could not be reproduced even qualitatively, which would be fatal for the analysis of the polarization of the optical spectra. This is due to the octahedral approximation and the neglect of the off-diagonal elements for the matrix elements of  $h$ . Since the explicit form of  $h$  has been already obtained by Watanabe and Kamimura for the case of the classical  $X\alpha$  potential,<sup>20</sup> we also calculated the multiplet structure of ruby using their formula.<sup>21</sup> This approach is referred to as the direct matrix calculation (DMC) approach in the present paper. Then the qualitative behavior of the trigonal-field splits of the quartets was reproduced and the degeneracy of each state was significantly improved, implying that the configuration interactions were taken into account more appropriately. However, in the DMC approach, the absolute energies of the quartets were significantly overestimated implying that the form of the exchange-correlation part of  $h$  is not the best. Therefore an improvement of  $h$  using a more sophisticated theoretical approach such as generalized gradient approximation (GGA) (Refs. 22–24) would be quite necessary. However, unfortunately an improved form of  $h$  has not been obtained yet. Instead, in the present paper, we propose a more efficient approach by combining the advantages of the FCZ approach with those of the DMC approach. In this approach, a configuration-dependent correction (CDC) is introduced and added to the matrix elements of the present DMC approach. These corrections are estimated by a method similar to the FCZ approach. The multiplet structure of ruby has been also calculated by this CDC approach and both the absolute energies and the trigonal splits of the quartets were reproduced satisfactorily.

Next, we consider the effect of electron correlations. In our previous calculation, the calculated multiplet energies were somewhat overestimated especially in the doublets due

to the underestimation of the effect of electron correlations. In principle, electron correlations can be systematically taken into account through the CI calculation with sufficient amount of Slater determinants as basis functions. In our previous calculation, however, the Slater determinants consisting only of the impurity-state orbitals were considered. Therefore the subspace for the diagonalization of the many-electron Hamiltonian was not sufficient to describe the effect of electron correlations accurately. However, since the basic multiplet structure can be reproduced even by such a limited calculation, the remaining effect of electron correlations is quite simple: a reduction of the electron-electron repulsion integrals. In spite of the simplicity of the physical image, it is generally quite inefficient to accomplish the remaining corrections only by the CI calculations. Therefore, instead of performing such intensive calculations, the effect of electron correlations has been frequently taken into account by introducing a certain reduction factor to be multiplied on the electron-electron repulsion integrals. For example, de Groot *et al.* calculated the multiplet structures appearing in the core excitation spectra of several TM compounds using atomic multiplet approach.<sup>25</sup> In their calculation, a suitable reduction factor was introduced and multiplied on the Slater integrals. In this case, the reduction factor includes both the effect of covalency and the effect of electron correlations.

In the present work, we also introduced a certain reduction factor to be multiplied on the electron-electron repulsion integrals. Since the effect of covalency is already included in the electron-electron repulsion integrals calculated by the molecular orbitals, the remaining correction is the effect of electron correlations. Therefore we call it the correlation correction (CC) factor. For the theoretical prediction of the multiplet structure, the CC factor should be estimated without referring to any experimental data. Considering the fact that electron correlations are partly included within the single-electron calculation based on DFT, we estimated the CC factor from the consistency between the DFT calculation and the multiplet calculation. In this method, not only the spin-restricted DFT calculation but also the spin-unrestricted DFT calculation is combined with the CI calculation. Therefore, in the present paper, this approach is referred to as the DFT-CI approach so that it can be distinguished from the previous SRDFT-CI approach. By the calculation based on the DFT-CI approach, the multiplet structures of ruby and  $\alpha\text{-Al}_2\text{O}_3:\text{V}^{3+}$  were reproduced quite satisfactorily without referring to any experimental data and the effect of electron correlation as well as the effect of covalency were evaluated quantitatively.

In the DFT-CI calculation, the many-electron wave functions are explicitly obtained as linear combination of the Slater determinants. Therefore a direct calculation of various physical quantities such as transition probability is possible. In the TM-doped  $\alpha\text{-Al}_2\text{O}_3$ , an impurity TM ion is octahedrally coordinated by six oxygen ions. However, this oxygen octahedron is trigonally distorted. As a result, the electric-dipole transition is slightly allowed and contribute to the absorption spectra. Therefore, in the present work, the intensities of the electric-dipole transition in ruby and  $\alpha\text{-Al}_2\text{O}_3:\text{V}^{3+}$  have been calculated numerically using the trigonally distorted many-electron wave functions. The calculated intensities reproduced the polarization of the absorp-

tion spectra of ruby qualitatively. In the case of  $\alpha\text{-Al}_2\text{O}_3:\text{V}^{3+}$ , a similar calculation could not reproduce the polarization of the  ${}^3T_2$  state, implying the importance of the other effects such as the spin-orbit interaction or the dynamic Jahn-Teller effect.

## II. DETAILS OF THE CALCULATION

### A. Hamiltonian of the impurity electrons

In the present calculation, only the electrons occupying the impurity states are considered explicitly. Thus, instead of the exact Hamiltonian for all electrons in the system, we consider an effective Hamiltonian,

$$H = \sum_{i=1}^M h(\mathbf{r}_i) + \sum_i \sum_{j<i} g(\mathbf{r}_i, \mathbf{r}_j), \quad (2.1)$$

where  $\mathbf{r}_i$  is the position of the  $i$ th electron and  $M$  is the number of electrons occupying the impurity states. The first and the second terms of  $H$  represent one-electron operators and two-electron operators, respectively. The one-electron operator consists of the kinetic energy, the Coulomb potential from the nuclei,  $V_{\text{ext}}(\mathbf{r})$ , and the Coulomb repulsion energy from the core and valence electrons,  $V_0(\mathbf{r})$ ,

$$h(\mathbf{r}) = -\frac{1}{2}\nabla^2 + V_{\text{ext}}(\mathbf{r}) + V_0(\mathbf{r}). \quad (2.2)$$

On the other hand, the two-electron operator represents the Coulomb repulsion interaction between the electrons occupying the impurity states

$$g(\mathbf{r}_i, \mathbf{r}_j) = \frac{1}{r_{ij}}, \quad (2.3)$$

where  $r_{ij}$  is the distance between the  $i$ th electron and the  $j$ th electron. This effective many-electron Hamiltonian  $H$  is then diagonalized within the subspace spanned by the Slater determinants  $\Phi_i$  constructed from the impurity-state orbitals obtained by the single-electron cluster calculation. The matrix elements of  $H$  can be generally expanded as

$$H_{pq} = \langle \Phi_p | H | \Phi_q \rangle = \sum_{i=1}^L \sum_{j=1}^L A_{ij}^{pq} \langle i | h | j \rangle + \sum_{i=1}^L \sum_{j=1}^L \sum_{k=1}^L \sum_{l=1}^L B_{ijkl}^{pq} \langle ij | g | kl \rangle, \quad (2.4)$$

where  $L$  is the number of the impurity-state orbitals and  $A_{ij}^{pq}$  and  $B_{ijkl}^{pq}$  are coefficients. Here,  $\langle i | h | j \rangle$  and  $\langle ij | g | kl \rangle$  are defined by

$$\langle i | h | j \rangle = \int \phi_i^*(\mathbf{r}) h(\mathbf{r}) \phi_j(\mathbf{r}) d\mathbf{r}, \quad (2.5)$$

and

$$\langle ij | g | kl \rangle = \iint \phi_i^*(\mathbf{r}_1) \phi_j^*(\mathbf{r}_2) \frac{1}{r_{12}} \phi_k(\mathbf{r}_1) \phi_l(\mathbf{r}_2) d\mathbf{r}_1 d\mathbf{r}_2, \quad (2.6)$$

respectively, where  $\phi$  are the impurity-state orbitals obtained by the cluster calculation. By diagonalizing this matrix, the

eigenvectors ( $a_{n1}, a_{n2}, \dots, a_{nK}$ ) are obtained and the many-electron wave functions  $\Psi_n$  are expressed as linear combination of the Slater determinants,

$$\Psi_n = a_{n1}\Phi_1 + a_{n2}\Phi_2 + \dots + a_{nK}\Phi_K, \quad (2.7)$$

where  $K$  is the number of the Slater determinants. Therefore the energy of the  $n$ th eigenstate is expressed as

$$E^n = \langle \Psi_n | H | \Psi_n \rangle = \sum_p \sum_q^K a_{np}^* a_{nq} H_{pq}, \quad (2.8)$$

in terms of the matrix elements of  $H$  and the eigenvectors.

### B. Single-electron calculation

The single-electron cluster calculation was carried out self-consistently based on the local density-functional approach. For comparison, two types of the exchange-correlation potential were adopted: One was the Slater's  $X\alpha$  potential<sup>26</sup> with  $\alpha=0.7$  and the other was the local-spin-density approximation (LSDA) potential proposed by Vosko, Wilk, and Nusair.<sup>27,28</sup> The molecular orbitals were constructed as a linear combination of the numerically generated atomic orbitals (NAO). The NAO's were refined flexibly to the chemical environment in each iteration. All integrations were carried out numerically using pseudorandom sampling points.<sup>29</sup> The details of this program have been described by Adachi *et al.*<sup>30</sup> Since all electrons including core electrons are treated explicitly, this program has been applied for the analysis of core-excitation spectra for various oxides.<sup>31-34</sup> The spectral features as well as the absolute transition energy have been well reproduced and the peaks in the spectra were clearly explained and classified in terms of the chemical bonding state. This program has also been used to clarify the chemical bondings in various TM compounds.<sup>35,36</sup>

### C. Fazio-Caldas-Zunger (FCZ) approach

For the calculation of the matrix elements of the effective many-electron Hamiltonian  $H$ , the explicit form of  $V_0(\mathbf{r})$  is required. Although the analytical form of this potential was given by Watanabe and Kamimura in the case of the classical  $X\alpha$  potential,<sup>20</sup> a more efficient computational method has been proposed by Fazio, Caldas, and Zunger.<sup>18,19</sup> In this method, all single-electron mean-field effects are formally separated from the many-electron effects. Both of these effects can be calculated without knowing the explicit form of  $V_0(\mathbf{r})$  as explained below.

In the octahedral approximation, the Slater determinants constructed from the impurity states can be classified according to the number of electrons occupying the  $t_{2g}$  and  $e_g$  states ( $m$  and  $n$ ). Then the diagonal matrix element of the  $i$ th Slater determinant belonging to the  $(t_{2g})^m(e_g)^n$  configuration, or  $(m, n)$  configuration for simplicity, is expressed as

$$E(m, n; i) = \hat{E}(m, n) + \Delta E(m, n; i), \quad (2.9)$$

where  $\hat{E}(m, n)$  is the average energy of all Slater determinants belonging to the  $(m, n)$  configuration and  $\Delta E(m, n; i)$  is the deviation of  $E(m, n; i)$  from  $\hat{E}(m, n)$ . The value of  $\hat{E}(m, n)$  relative to another configuration,  $(m', n')$  corre-

sponds to the total-energy difference between these two configurations. Therefore it can be well approximated by the single-electron energy difference calculated for the Slater's transition state.<sup>26</sup> As we have already pointed out, however, the difference in the single-electron energy between the ground state and the Slater's transition state is negligible in the present case.<sup>15</sup> Thus we have evaluated the total-energy difference by the single-electron energy difference in the ground state in practice. Then the energy difference between the adjacent configuration is generally expressed as

$$\hat{E}(m-1, n+1) - \hat{E}(m, n) = \Delta_{\text{eff}}, \quad (2.10)$$

where  $\Delta_{\text{eff}}$  is the effective crystal-field split defined as the difference between the energies of  $t_{2g}$  and  $e_g$  states,

$$\Delta_{\text{eff}} = \varepsilon_e - \varepsilon_t. \quad (2.11)$$

Then the average energy of the  $(m, n)$  configuration relative to the  $(m+n, 0)$  configuration can be simply expressed as

$$\hat{E}(m, n) = n\Delta_{\text{eff}}. \quad (2.12)$$

In the FCZ approach, the matrix elements of Eq. (2.4) are approximated by

$$H_{pq} = D(m, n)\delta_{pq} + \sum_{i=1}^L \sum_{j=1}^L \sum_{k=1}^L \sum_{l=1}^L B_{ijkl}^{pq} \langle ij|g|kl \rangle, \quad (2.13)$$

where the matrix elements of  $\Sigma h$  are replaced by  $D(m, n)\delta_{pq}$ . In order to determine the value of  $D(m, n)$  for each configuration, the contribution of the average value of the electron-electron interaction term should be subtracted. This procedure can be accomplished by setting the average energy of the  $(m, n)$  configuration to be  $n\Delta_{\text{eff}}$ ,

$$\frac{1}{N(m, n)} \sum_{p \in (m, n)} H_{pp} = n\Delta_{\text{eff}}, \quad (2.14)$$

where  $N(m, n)$  is the number of the Slater determinants belonging to the  $(m, n)$  configuration and the sum of  $p$  is taken over all these Slater determinants. In this method, the off-diagonal matrix elements of  $\Sigma h$  are completely neglected and the diagonal elements are estimated in the octahedral approximation.

#### D. Direct matrix calculation (DMC) approach

The explicit form of  $V_0(\mathbf{r})$  in the effective single-electron Hamiltonian has already been derived by Watanabe and Kamimura for the case of the  $X\alpha$  potential as

$$\begin{aligned} V_0(\mathbf{r}) = & \int \frac{\rho_0^G(\mathbf{r}')}{|\mathbf{r}-\mathbf{r}'|} d\mathbf{r}' \\ & + \frac{3}{4} \left[ \frac{\rho^G(\mathbf{r})V_{xc}\{\rho^G(\mathbf{r})\} - \rho_0^G(\mathbf{r})V_{xc}\{\rho_0^G(\mathbf{r})\}}{\rho_{\text{imp}}^G(\mathbf{r})} \right. \\ & \left. - V_{xc}\{\rho_{\text{imp}}^G(\mathbf{r})\} \right], \quad (2.15) \end{aligned}$$

where  $\rho^G$ ,  $\rho_{\text{imp}}^G$ , and  $\rho_0^G$  represent the charge density of all electrons, that of the electrons occupying the impurity states,

and that of the remaining electrons, respectively, and  $V_{xc}$  is the Slater's  $X\alpha$  potential. The superscript  $G$  indicates the values in the ground state. In the direct matrix calculation (DMC) approach, the matrix elements of the effective single-electron Hamiltonian are calculated by Eq. (2.4) using  $V_0(\mathbf{r})$  defined by Eq. (2.15). Because the molecular orbitals used in the Slater determinants are eigenfunctions of the ordinary single-electron Hamiltonian in the local-density approximation (LDA),

$$h_{\text{LDA}}(\mathbf{r}) = -\frac{1}{2}\nabla^2 + V_{\text{ext}}(\mathbf{r}) + \int \frac{\rho(\mathbf{r}')}{|\mathbf{r}-\mathbf{r}'|} d\mathbf{r}' + V_{xc}\{\rho(\mathbf{r})\}, \quad (2.16)$$

the off-diagonal matrix elements of  $\Sigma h(\mathbf{r})$  are not necessarily zero, although they are completely neglected in the FCZ approach. In the DMC approach, these off-diagonal elements are calculated directly and the configuration interactions among the Slater determinants can be evaluated more appropriately.

#### E. Configuration-dependent correction (CDC) approach

In our previous calculation, we found that the FCZ approach was effective for the prediction of the average energy of each state in the  $O_h$  notation, however, the trigonal-field splits could not be described properly.<sup>21</sup> This is due to the octahedral approximation and the neglect of the off-diagonal elements for the matrix elements of  $\Sigma h$ . On the other hand, the DMC method describes the trigonal-field splits properly, but significantly overestimates the absolute energies of the multiplets, implying that the expression of  $V_0(\mathbf{r})$  defined by Eq. (2.15) is not the best. Although an improvement of the expression of  $V_0(\mathbf{r})$  using a more sophisticated approach such as GGA (Refs. 22–24) is quite important, it has not been accomplished yet. Considering that the absolute energy of the multiplets can be well evaluated by the FCZ approach, it is natural to apply a similar configuration-dependent correction (CDC) technique to the matrix element of the DMC approach. In this CDC approach, the matrix elements of the Hamiltonian ( $H'_{pq}$ ) are expressed as

$$H'_{pq} = H_{pq} + D_{\text{CDC}}(m, n)\delta_{pq}, \quad (2.17)$$

where  $D_{\text{CDC}}(m, n)$  is the correction to the matrix elements of  $\Sigma h$  for the states belonging to the  $(m, n)$  configuration. The values of  $D_{\text{CDC}}(m, n)$  are determined from Eq. (2.14) as in the case of the FCZ approach by inserting  $H'_{pp}$  instead of  $H_{pp}$ .

#### F. Correlation correction factor

In the present calculation, only the impurity-state orbitals are used for the construction of the Slater determinants. Therefore the number of the Slater determinants is not sufficient to describe the effect of electron correlations accurately. Since the basic multiplet structure can be obtained even by such a limited calculation, the remaining effect of electron correlations is a reduction of the effective electron-electron repulsion energy. In the present work, we introduce a correlation correction factor  $c$  and define the effective electron-electron repulsion integrals by

$$\langle ij|g|kl\rangle_{\text{eff}} = c\langle ij|g|kl\rangle. \quad (2.18)$$

The matrix elements of the many-electron Hamiltonian are calculated using these effective electron-electron repulsion integrals. Considering the fact that electron correlations are partly included within the spin-unrestricted single-electron DFT calculation, we tentatively determined the value of  $c$ , from the consistency between the single-electron DFT calculation and the many-electron multiplet calculation. This procedure can be formulated as follows.

In the density-functional formalism, the ground-state energy of an  $N$ -electron system  $E_N$  can be written in terms of the ground-state charge density  $\rho^G(\mathbf{r})$  and the potential due to the nuclei  $V_{\text{ext}}(\mathbf{r})$ , as

$$\begin{aligned} E_N^G &= T[\rho^G(\mathbf{r})] + \int \rho^G(\mathbf{r})V_{\text{ext}}(\mathbf{r})d\mathbf{r} \\ &+ \frac{1}{2} \int \int \frac{\rho^G(\mathbf{r})\rho^G(\mathbf{r}')}{|\mathbf{r}-\mathbf{r}'|} d\mathbf{r}d\mathbf{r}' + E_{\text{ex}}[\rho^G(\mathbf{r})]. \end{aligned} \quad (2.19)$$

Here the first, second, third, and last terms represent the kinetic energy, the potential energy due to  $V_{\text{ext}}(\mathbf{r})$ , the Coulomb repulsion energy, and the exchange-correlation energy. In the present calculation, we consider only electrons occupying the impurity states. Thus we divide  $E_N^G$  into two parts,

$$E_N^G = E_0^G + E_{\text{imp}}^G, \quad (2.20)$$

where  $E_0^G$  is a part related only to the charge density of the core and valence electrons  $\rho_0^G(\mathbf{r})$ ,

$$\begin{aligned} E_0^G &= T[\rho_0^G(\mathbf{r})] + \int \rho_0^G(\mathbf{r})V_{\text{ext}}(\mathbf{r})d\mathbf{r} \\ &+ \frac{1}{2} \int \int \frac{\rho_0^G(\mathbf{r})\rho_0^G(\mathbf{r}')}{|\mathbf{r}-\mathbf{r}'|} d\mathbf{r}d\mathbf{r}' + E_{\text{ex}}[\rho_0^G(\mathbf{r})], \end{aligned} \quad (2.21)$$

and  $E_{\text{imp}}^G$  is a part related to the charge density of the electrons occupying the impurity states  $\rho_{\text{imp}}^G(\mathbf{r})$ ,

$$\begin{aligned} E_{\text{imp}}^G &= T[\rho_{\text{imp}}^G(\mathbf{r})] + \int \rho_{\text{imp}}^G(\mathbf{r})V_{\text{ext}}(\mathbf{r})d\mathbf{r} \\ &+ \frac{1}{2} \int \int \frac{\rho_{\text{imp}}^G(\mathbf{r})\rho_{\text{imp}}^G(\mathbf{r}')}{|\mathbf{r}-\mathbf{r}'|} d\mathbf{r}d\mathbf{r}' \\ &+ \int \int \frac{\rho_{\text{imp}}^G(\mathbf{r})\rho_0^G(\mathbf{r}')}{|\mathbf{r}-\mathbf{r}'|} d\mathbf{r}d\mathbf{r}' + E_{\text{ex}}[\rho_{\text{imp}}^G(\mathbf{r})] \\ &- E_{\text{ex}}[\rho_0^G(\mathbf{r})]. \end{aligned} \quad (2.22)$$

Now we compare this result with the eigenvalue of the effective many-electron Hamiltonian  $H$ . As we have already mentioned, in the eigenenergy expressed by Eq. (2.8), the effect of electron correlations is underestimated due to the insufficiency of the number of the Slater determinants. However, the remaining effect of electron correlations can be taken into account by introducing the CC factor  $c$  to be multiplied on the electron-electron repulsion integrals. Then the

matrix elements of the effective many-electron Hamiltonian can be expressed as a function of  $c$ :

$$\begin{aligned} H_{pq}(c) &= \sum_{i=1}^L \sum_{j=1}^L A_{ij}^{pq} \langle i|h|j\rangle + \sum_{i=1}^L \sum_{j=1}^L \sum_{k=1}^L \sum_{l=1}^L c \\ &\times B_{ijkl}^{pq} \langle ij|g|kl\rangle. \end{aligned} \quad (2.23)$$

Since the eigenvectors are obtained by diagonalizing this matrix, the many-electron wave functions also depend on  $c$ ,

$$\Psi_n(c) = a_{n1}(c)\Phi_1 + a_{n2}(c)\Phi_2 + \cdots + a_{nK}(c)\Phi_K. \quad (2.24)$$

Accordingly the eigenenergy of the  $n$ th state also depend on  $c$ ,

$$E^n(c) = \sum_p^K \sum_q^K a_{np}^*(c)a_{nq}(c)H_{pq}(c). \quad (2.25)$$

With the appropriate value of  $c$ , the eigenenergy of the ground state coincides with that obtained by the density-functional approach,

$$E^G(c) = E_{\text{imp}}^G. \quad (2.26)$$

The consideration of this CC factor  $c$  is equivalent to an approximation using the following effective Hamiltonian instead of  $H$  defined by Eq. (2.1):

$$H' = \sum_{i=1}^M h(\mathbf{r}_i) + \sum_i \sum_{j<i} g'(\mathbf{r}_i, \mathbf{r}_j), \quad (2.27)$$

where  $h(\mathbf{r})$  is the same as Eq. (2.2) and  $g'(\mathbf{r}_i, \mathbf{r}_j)$  is defined by

$$g'(\mathbf{r}_i, \mathbf{r}_j) = \frac{c}{r_{ij}}. \quad (2.28)$$

In other words, the electron-electron repulsion integrals are reduced uniformly in this approximation.

Although the value of  $c$  can be evaluated by Eq. (2.26), the accuracy of the total-energy calculation is rather uncertain. In the present work, we have developed a more effective method to evaluate the value of  $c$  from first principles, using a spin-flip excitation within the states consisting of the same spatial orbitals. For example, we consider a case of three impurity electrons in the  $O_h$  symmetry. In this case, the ground state and the spin-flip excited state can be expressed as  $(t_{2g} \uparrow)^3$  and  $(t_{2g} \uparrow)^2(t_{2g} \downarrow)^1$ , respectively. In the local-density-functional formalism, the energy difference between these states can be expressed as

$$E_N^E - E_N^G = \varepsilon_{t_{2g} \downarrow}^{TS} - \varepsilon_{t_{2g} \uparrow}^{TS}, \quad (2.29)$$

where  $E_N^G$  is the total energy of the  $(t_{2g} \uparrow)^3$  configuration and  $E_N^E$  is the total energy of the  $(t_{2g} \uparrow)^2(t_{2g} \downarrow)^1$  configuration, while  $\varepsilon_{t_{2g} \downarrow}^{TS}$  and  $\varepsilon_{t_{2g} \uparrow}^{TS}$  are single-electron orbital energies for the  $t_{2g} \downarrow$  and  $t_{2g} \uparrow$  states calculated in the  $(t_{2g} \uparrow)^{2.5}(t_{2g} \downarrow)^{0.5}$  configuration. As we have shown in Eq. (2.20),  $E_N^G$  ( $E_N^E$ ) can be divided into two parts,

$$\begin{cases} E_N^G = E_0^G + E_{\text{imp}}^G \\ E_N^E = E_0^E + E_{\text{imp}}^E \end{cases} \quad (2.30)$$

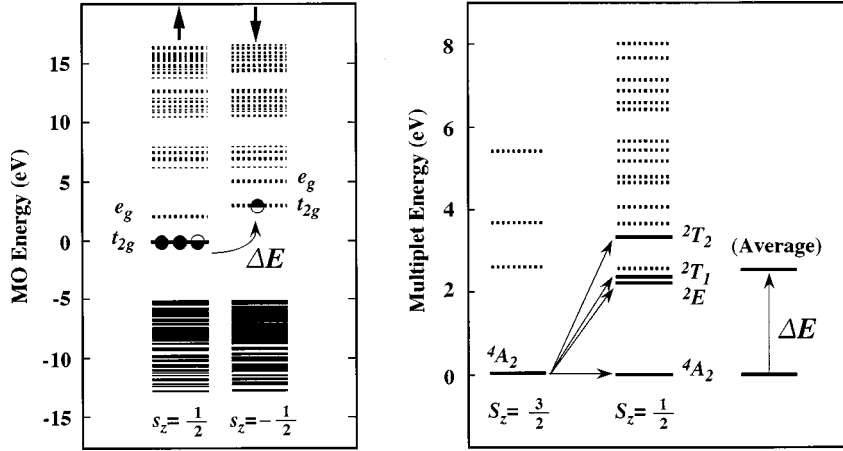


FIG. 1. Schematic illustrations of the spin-flip transition energy  $\Delta E$  within the  $(t_{2g})^3$  configuration in the  $O_h$  symmetry ( $S_z = \frac{3}{2} \rightarrow S_z = \frac{1}{2}$ ) in terms of the single-electron energy level (left) and in terms of the multiplet energy level (right), where  $s_z$  denotes the  $z$  component of the spin of each electron and  $S_z$  denotes the  $z$  component of the total spin.

where  $E_0^G$  ( $E_0^E$ ) is a part related only to the core and valence electrons while  $E_{\text{imp}}^G$  ( $E_{\text{imp}}^E$ ) is a part related to the electrons occupying the impurity states. Since the  $(t_{2g} \uparrow)^3$  and  $(t_{2g} \uparrow)^2(t_{2g} \downarrow)^1$  states consist of the same spatial orbitals, we neglect the relaxation of the core and valence electrons during the transition ( $E_0^G \sim E_0^E$ ). Therefore we can drop these terms from Eq. (2.29) and obtain

$$E_{\text{imp}}^E - E_{\text{imp}}^G = \varepsilon_{t_{\downarrow}}^{TS} - \varepsilon_{t_{\uparrow}}^{TS}. \quad (2.31)$$

Moreover,  $E_{\text{imp}}^G$  ( $E_{\text{imp}}^E$ ) is equal to the corresponding eigenvalue of  $H$  when the appropriate CC factor  $c^G$  ( $c^E$ ) is adopted,

$$\begin{cases} E^G(c^G) = E_{\text{imp}}^G \\ E^E(c^E) = E_{\text{imp}}^E \end{cases} \quad (2.32)$$

Here we also assume that the difference between  $c^G$  and  $c^E$  is negligible, since the  $(t_{2g} \uparrow)^3$  and  $(t_{2g} \uparrow)^2(t_{2g} \downarrow)^1$  states consist of the same spatial orbitals. By setting  $c^G = c^E = c$ , we obtain

$$E^E(c) - E^G(c) = \varepsilon_{t_{\downarrow}}^{TS} - \varepsilon_{t_{\uparrow}}^{TS}. \quad (2.33)$$

In the actual multiplet energy levels, several states may correspond to the spin-flip excited state. For example, the  $(t_{2g} \uparrow)^2(t_{2g} \downarrow)^1$  configuration corresponds to four different states,  ${}^2T_2$ ,  ${}^2T_1$ ,  ${}^2E$ , and  ${}^4A_2$  ( $S_z = \frac{1}{2}$ ) in the multiplet energy level, where  $S_z$  is the  $z$  component of the total spin. In such a case, we take gravity center of the corresponding states as the energy of the excited state,

$$E^E(c) = \frac{\sum_k g_k E_k^E(c)}{\sum_k g_k}, \quad (2.34)$$

where  $g_k$  is the degeneracy of the  $k$ th excited state. Finally, we obtain

$$\frac{\sum_k g_k E_k^E(c)}{\sum_k g_k} - E^G(c) = \varepsilon_{t_{\downarrow}}^{TS} - \varepsilon_{t_{\uparrow}}^{TS}. \quad (2.35)$$

In the present work, the value of  $c$  was determined by this equation.

The physical meaning of this equation is quite simple. For example, in the case of three impurity electrons in the  $O_h$  symmetry, we consider a spin-flip transition from  $S_z = \frac{3}{2}$  to  $S_z = \frac{1}{2}$  within the  $(t_{2g})^3$  configuration. This transition corresponds to the transition from  $t_{2g} \uparrow$  to  $t_{2g} \downarrow$  in terms of the spin-unrestricted single-electron energy level and the transition energy can be calculated by the Slater's transition state method. On the other hand, the same transition corresponds to the transitions from  ${}^4T_2$  ( $S_z = \frac{3}{2}$ ) to four different states,  ${}^2T_2$ ,  ${}^2T_1$ ,  ${}^2E$ , and  ${}^4A_2$  ( $S_z = \frac{1}{2}$ ) in terms of the multiplet energy level. The two different descriptions are schematically shown in Fig. 1.

### G. Transition probability

An impurity TM ion in  $\alpha\text{-Al}_2\text{O}_3$  is octahedrally coordinated by six oxygen ions. This oxygen octahedron is trigonally distorted, and the electric-dipole transitions are slightly allowed. The multiplet energies of these materials are frequently analyzed in the octahedral approximation. However, such calculations cannot predict the transition probabilities between the multiplets directly, since the electric-dipole transition between these multiplets are strictly forbidden in the octahedral approximation. In the present work, the trigonally distorted many-electron wave functions are obtained explicitly using the trigonally distorted molecular orbitals obtained by the cluster calculation. Therefore the transition probability of the electric-dipole transition between the multiplets can be calculated directly. The oscillator strength of the electric-dipole transition can be calculated by<sup>1</sup>

$$I_{if} = 2(E_f - E_i) \left| \left\langle \Psi_i \left| \sum \mathbf{r}_k \cdot \mathbf{e} \right| \Psi_f \right\rangle \right|^2 \quad (2.36)$$

where  $\Psi_i$  and  $\Psi_f$  are the many-electron wave functions of the initial and final states, while  $E_i$  and  $E_f$  are the energy eigenvalues of these states.  $\mathbf{r}_k$  denotes the position of the  $k$ th electron and  $\mathbf{e}$  denotes the unit vector parallel to the direction of the electric field.

### H. Model clusters

In order to determine the appropriate cluster size for the present investigation, we considered three clusters of differ-

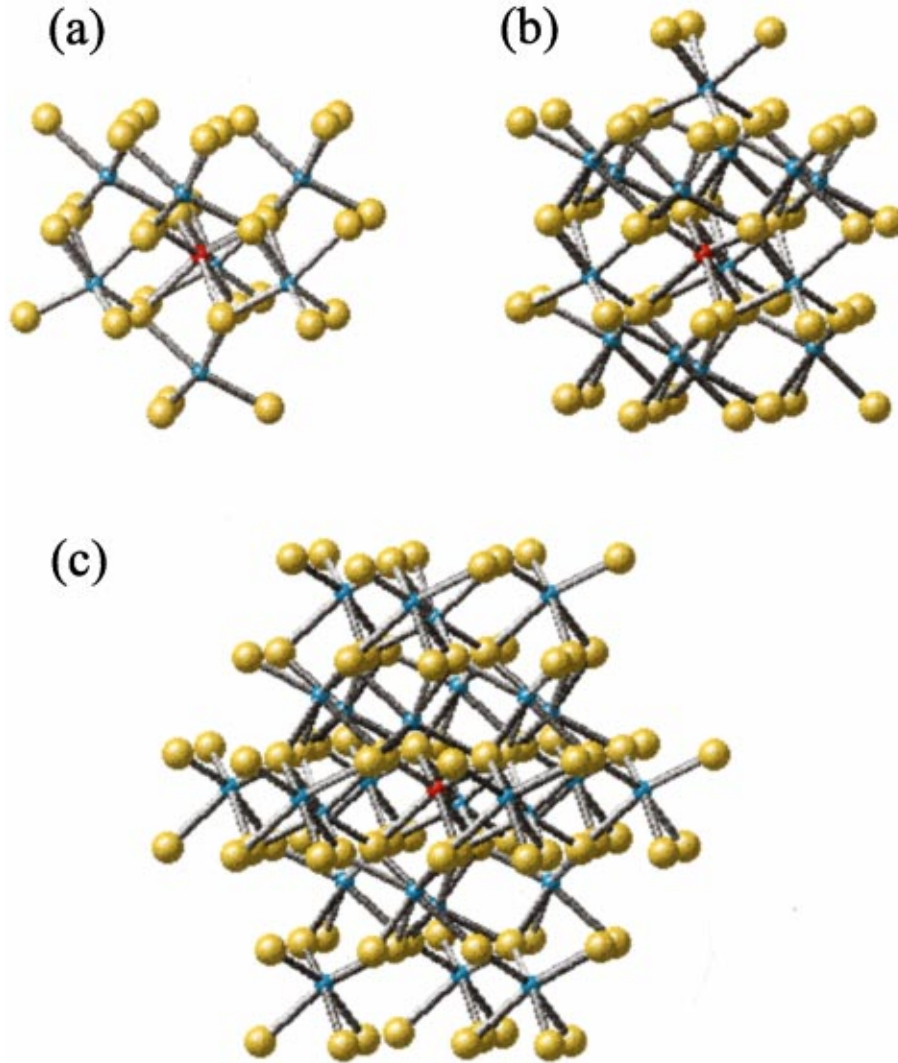


FIG. 2. (Color) Model clusters for the transition-metal (TM) doped  $\alpha\text{-Al}_2\text{O}_3$  consisting of (a) 41, (b) 63, and (c) 111 atoms. The small red sphere, small blue sphere, and large yellow sphere denote TM ions, aluminum ions, and oxygen ions, respectively.

ent size as shown in Fig. 2. The clusters (a), (b), and (c) consist of 41, 63, and 111 atoms, respectively. These clusters were constructed based on the crystal data of  $\alpha\text{-Al}_2\text{O}_3$  and approximately 4000 point charges were located at the external atomic sites so as to reproduce the effective Madelung potential. The TM ion was located at the center of each cluster. In the clusters (a), (b), and (c), 7, 14, and 26 aluminum ions were included, respectively, and all of the first-neighbor six oxygen ions to these aluminum ions were taken into account. Basis sets used in the present calculations were  $1s\text{-}2p$  for oxygen,  $1s\text{-}3d$  for aluminum, and  $1s\text{-}4p$  for chromium or vanadium. Numerical integrations were carried out using 30 000, 40 000, and 80 000 sampling points for the clusters (a), (b), and (c), respectively.

### III. SINGLE-ELECTRON ENERGY LEVELS

#### A. Cluster size dependence

The calculated spin-restricted single-electron energy levels of ruby using the clusters (a), (b), and (c) are shown in Fig. 3, where the energies of the highest occupied molecular orbitals are set at zero. All calculations were carried out us-

ing the Slater's  $X\alpha$  potential. The valence band mainly consists of the O- $2p$  orbitals and the conduction band mainly consists of the Al- $3s$ ,  $3p$ ,  $3d$  orbitals. There are impurity states corresponding to the  $t_{2g}$  and  $e_g$  states in the  $O_h$  notation, mainly consisting of the  $3d$  orbitals of the impurity chromium ion. Due to the presence of the trigonal crystal field, the  $t_{2g}$  state further splits into the states with  $a$  and  $e$  symmetry. If we define the effective crystal-field split  $\Delta_{\text{eff}}$  as the difference between the energy of the  $e_g$  state and the average energy of the  $t_{2g}$  state, the calculated values of  $\Delta_{\text{eff}}$  are 2.12, 2.11, and 2.12 eV for the clusters (a), (b), and (c), respectively. Therefore the variation of  $\Delta_{\text{eff}}$  is quite small. The trigonal splits of the  $t_{2g}$  state,  $\varepsilon_{i(a)} - \varepsilon_{i(e)}$ , are  $-0.04$ ,  $0.03$ , and  $0.06$  eV for the clusters (a), (b) and (c), respectively. Therefore the positions of  $t_{2g}(a)$  and  $t_{2g}(e)$  are reversed between the cluster (a) and the cluster (b), while the results of the cluster (b) and the cluster (c) are qualitatively consistent. As the number of atoms in the cluster is increased, the widths of the valence band and the conduction band become slightly broader. The relative position of the impurity states from the top of the valence band slightly changes between the cluster (a) and the cluster (b), while

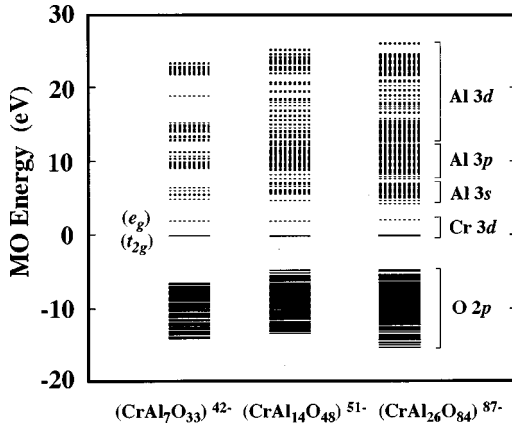


FIG. 3. The spin-restricted molecular orbital (MO) energy levels of ruby calculated using the clusters  $(\text{CrAl}_7\text{O}_{33})^{42-}$  (left),  $(\text{CrAl}_{14}\text{O}_{48})^{51-}$  (center), and  $(\text{CrAl}_{26}\text{O}_{84})^{87-}$  (right). The energies of the highest occupied molecular orbitals are set at zero. The solid lines denote the occupied states and the dotted lines denote the unoccupied states.

there is no significant change between the cluster (b) and the cluster (c). Therefore the electronic structure around the impurity states is almost the same between the cluster (b) and the cluster (c). In order to confirm this result, we also investigated the composition of the Cr-3d orbitals within the impurity-state orbitals by the Mulliken population analysis<sup>37</sup> as listed in Table I. As shown in the table, the Cr-3d compositions at the  $t_{2g}(a)$ ,  $t_{2g}(e)$ , and  $e_g$  states change 1.4, 1.6, and 2.8%, respectively, between the cluster (a) and the cluster (b). On the other hand, the change of the Cr-3d composition in each orbital is within 0.2% between the cluster (b) and the cluster (c). Thus we conclude that the impurity-state orbitals are well described by the cluster (b) and the calculations of the multiplet structures of ruby and  $\alpha\text{-Al}_2\text{O}_3:\text{V}^{3+}$  were carried out using the cluster (b) in the present work.

### B. Exchange-correlation potential dependence

The spin-restricted density functional calculation for the  $(\text{CrAl}_{14}\text{O}_{48})^{51-}$  cluster was also carried out using the LSDA potential. The results are shown in Fig. 4, together with the results using the  $X\alpha$  potential. In this figure, the top of the valence bands are set at zero. The calculated effective crystal-field splits  $\Delta_{\text{eff}}$  are 2.12 and 2.11 eV for the LSDA potential and the  $X\alpha$  potential, respectively. According to the Mulliken population analysis,<sup>37</sup> the change in the composition of the impurity-state orbitals between these calculations is negligibly small. For example, the change of the Cr-3d composition in each orbital is less than 0.03%. These results indicate that for a spin-restricted calculation, the result using the  $X\alpha$  potential and that using the LSDA potential are es-

TABLE I. Composition of the Cr-3d orbitals within each impurity-state orbital (%) obtained by the three different clusters.

	$t_{2g}(a)$	$t_{2g}(e)$	$e_g(e)$
$(\text{CrAl}_7\text{O}_{33})^{42-}$	91.5	92.9	83.3
$(\text{CrAl}_{14}\text{O}_{48})^{51-}$	90.1	91.3	80.5
$(\text{CrAl}_{26}\text{O}_{84})^{87-}$	90.3	91.3	80.3

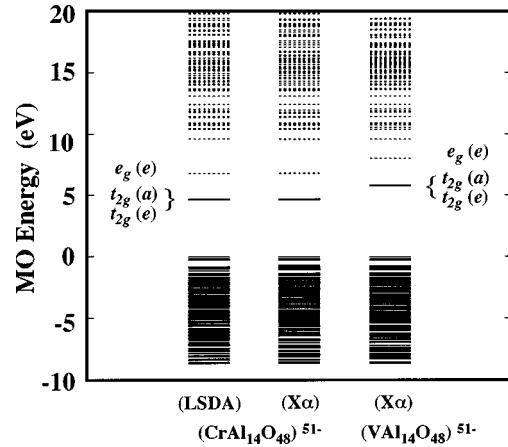


FIG. 4. The spin-restricted molecular-orbital (MO) energy levels of ruby calculated by the LSDA potential using the  $(\text{CrAl}_{14}\text{O}_{48})^{51-}$  cluster (left), those calculated by the  $X\alpha$  potential using the same cluster (center), and the spin-restricted MO energy levels of  $\alpha\text{-Al}_2\text{O}_3:\text{V}^{3+}$  calculated by the  $X\alpha$  potential using the  $(\text{VA}_{14}\text{O}_{48})^{51-}$  cluster (right). The energies of the top of the valence bands are set at zero. The solid lines denote the occupied states and the dotted lines denote the unoccupied states.

entially the same. Therefore, in the present work, the impurity-state orbitals obtained by the calculation using the  $X\alpha$  potential were used for the construction of the Slater determinants.

### C. Ruby and $\alpha\text{-Al}_2\text{O}_3:\text{V}^{3+}$

The single-electron energy level of the  $(\text{VA}_{14}\text{O}_{48})^{51-}$  cluster was also calculated using the  $X\alpha$  potential and compared with the result of the  $(\text{CrAl}_{14}\text{O}_{48})^{51-}$  cluster in Fig. 4. The positions of the impurity states are closer to the conduction band in  $\alpha\text{-Al}_2\text{O}_3:\text{V}^{3+}$  than in ruby. Therefore it is expected that the interaction between the TM-3d orbitals and the Al-3s, 3p, 3d orbitals is greater in  $\alpha\text{-Al}_2\text{O}_3:\text{V}^{3+}$  than in ruby while the interaction between the TM-3d orbitals and the O-2p orbitals is greater in ruby than in  $\alpha\text{-Al}_2\text{O}_3:\text{V}^{3+}$ . In ruby, these ten impurity states are occupied by three electrons. Therefore  ${}_{10}\text{C}_3$  (=120) Slater determinants were constructed and used as the basis functions for the diagonalization of the many-electron Hamiltonian. In the case of  $\alpha\text{-Al}_2\text{O}_3:\text{V}^{3+}$ , there are two impurity electrons and  ${}_{10}\text{C}_2$  (=45) Slater determinants were used as the basis functions.

As we have already mentioned, the value of  $\Delta_{\text{eff}}$  calculated using the  $(\text{CrAl}_{14}\text{O}_{48})^{51-}$  cluster using the  $X\alpha$  potential is 2.11 eV. This is much smaller than the value obtained by Duan *et al.*,<sup>12</sup> which is approximately 2.5 eV according to the Fig. 2 in their paper. The value of  $\Delta_{\text{eff}}$  is related to the energy of the U band in the optical spectra of ruby. As will be shown later, our calculation slightly overestimates the U-band energy. Therefore their value would further overestimate the U-band energy. In their calculation, the structural relaxation around the impurity chromium ion is considered. However, as will be discussed in Sec. IV C, the consideration of the relaxation would decrease the value of  $\Delta_{\text{eff}}$  due to the slightly longer Cr-O bond lengths. Therefore our results would further agree with the experimental data. The reason for this discrepancy is not clear.

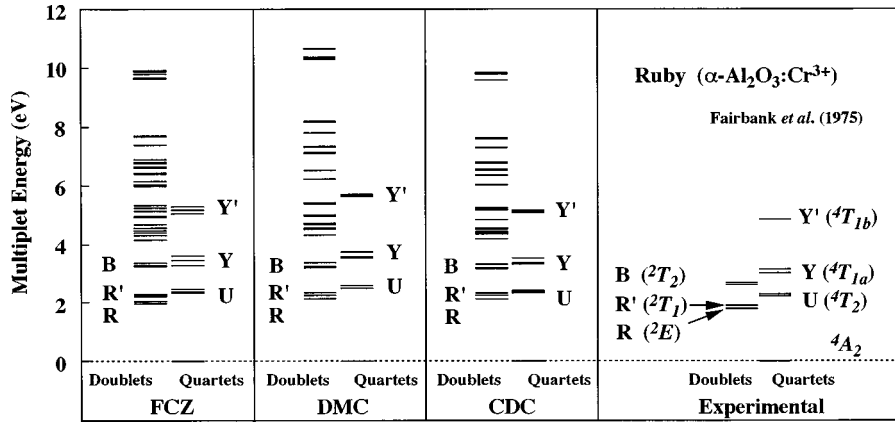


FIG. 5. The multiplier energy levels of ruby calculated by the three different approaches (FCZ, DMC, and CDC) using the  $(\text{CrAl}_{14}\text{O}_{48})^{51-}$  cluster with no correlation correction (NCC). The energy of the ground state ( ${}^4A_2$ ) is set at zero. The peak positions in the observed absorption spectra of ruby reported by Fairbank *et al.* (Ref. 9) are shown together on the right.

The effective crystal-field split and the trigonal-field split were also calculated for  $\alpha\text{-Al}_2\text{O}_3:\text{V}^{3+}$ . The value of  $\Delta_{\text{eff}}$  calculated using the  $(\text{VAl}_{14}\text{O}_{48})^{51-}$  cluster is 2.28 eV, which is slightly larger than the value for ruby (2.11 eV). The calculated value of the trigonal field split,  $\varepsilon_{t(a)} - \varepsilon_{t(e)}$ , is 0.02 eV, which is slightly smaller than the value for ruby (0.03 eV).

#### IV. MULTIPLLET STRUCTURE OF RUBY

##### A. Multiplier structure without CC

The multiplier structures of ruby ( $\alpha\text{-Al}_2\text{O}_3:\text{Cr}^{3+}$ ) calculated by the three different approaches (FCZ, DMC, and CDC) using the  $(\text{CrAl}_{14}\text{O}_{48})^{51-}$  cluster with no correlation correction (NCC) are shown in Fig. 5. The energy of the

ground state ( ${}^4A_2$ ) is set at zero. The peak positions in the absorption spectra of ruby reported by Fairbank *et al.*<sup>9</sup> are shown together on the right. Since the ground state is a quartet ( ${}^4A_2$ ), transitions to the quartets,  ${}^4T_2$ ,  ${}^4T_{1a}$ , and  ${}^4T_{1b}$  are allowed by the spin-selection rule and observed as strong and broad bands. Although transitions to the doublets,  ${}^2E$ ,  ${}^2T_1$ , and  ${}^2T_2$  are forbidden by the spin-selection rule, they are slightly allowed due to the presence of the spin-orbit interaction and observed as weak and sharp lines. Each peak slightly splits due to the trigonal crystal field (quartets) or due to the spin-orbit interaction (doublets) as listed in Table II. Since the splits due to the trigonal field are quite small, we mainly discuss the average energy of each state in the  $O_h$  notation for a while. The trigonal-field splits will be discussed in Sec. IV F with relation to the polarization of the

TABLE II. The multiplier energy levels of ruby (eV) calculated by the three different approaches (FCZ, DMC, and CDC), with no correlation correction (NCC) and with the correlation correction (CC), together with the peak positions in the observed absorption spectra of ruby reported by Fairbank *et al.* CC(LSDA) and CC( $X\alpha$ ) denote the calculations with the CC factors estimated by the single-electron calculations using the LSDA potential and the  $X\alpha$  potential, respectively. CC(expt) denote the calculation with the CC factor estimated from the experimental data. The calculated multiplier energies are averaged within each state in the  $O_h$  notation. For comparison, the results of Ohnishi and Sugano and those of Xia *et al.* are listed together.

			${}^2E(R)$	${}^2T_1(R')$	${}^2T_2(B)$	${}^4T_2(U)$	${}^4T_{1a}(Y)$	${}^4T_{1b}(Y')$
Experimental			1.79	1.85	2.60	2.23( $\sigma$ )	3.01( $\sigma$ )	4.84( $\sigma$ )
(Fairbank <i>et al.</i> <sup>a</sup> )			1.79	1.88	2.61	2.28( $\pi$ )	3.11( $\pi$ )	4.84( $\pi$ )
				1.88	2.65			
Ohnishi and Sugano <sup>b</sup>			1.63			2.27		
Xia <i>et al.</i> <sup>c</sup>			1.83 <sup>e</sup>			2.70		
$(\text{CrAl}_7\text{O}_{33})^{42-d}$	FCZ	NCC	2.23	2.37	3.45	2.47	3.52	5.28
$(\text{CrAl}_{14}\text{O}_{48})^{51-}$	FCZ	NCC	2.03	2.27	3.31	2.40	3.45	5.17
$(\text{CrAl}_{14}\text{O}_{48})^{51-}$	DMC	NCC	2.13	2.29	3.27	2.53	3.61	5.65
$(\text{CrAl}_{14}\text{O}_{48})^{51-}$	CDC	NCC	2.13	2.29	3.24	2.39	3.41	5.12
$(\text{CrAl}_{14}\text{O}_{48})^{51-}$	CDC	CC(LSDA)	1.35	1.49	2.24	2.28	3.04	4.73
$(\text{CrAl}_{14}\text{O}_{48})^{51-}$	CDC	CC( $X\alpha$ )	1.79	1.94	2.80	2.34	3.26	4.94
$(\text{CrAl}_{14}\text{O}_{48})^{51-}$	CDC	CC(expt)	1.71	1.85	2.69	2.33	3.22	4.89

<sup>a</sup>Reference 9.

<sup>b</sup>Reference 10.

<sup>c</sup>Reference 11.

<sup>d</sup>Reference 15.

<sup>e</sup>In the original paper of Xia *et al.*, the calculated spin-flip transition energy 2.29 eV was compared with the experimental data. However, according to the paper of Ohnishi and Sugano, this value should be multiplied by  $\frac{4}{3}$  to be compared with the  $R$ -line energy. Therefore the corrected value is listed here.

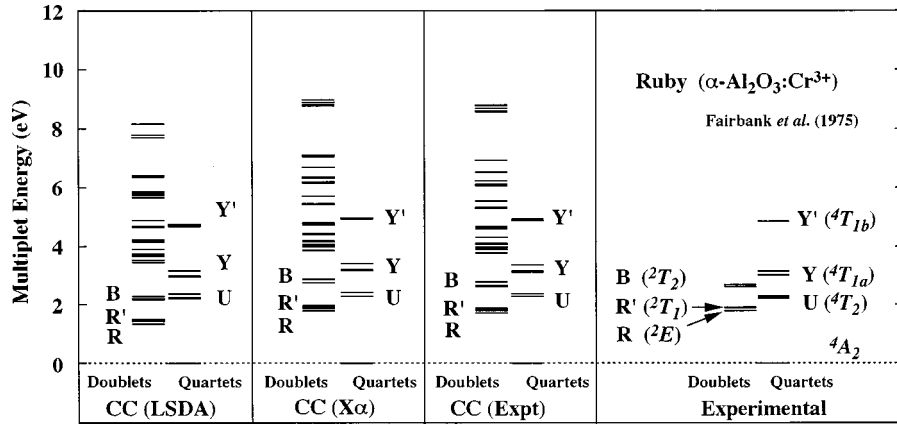


FIG. 6. The multiplet energy levels calculated by the CDC approach using the  $(\text{CrAl}_{14}\text{O}_{48})^{51-}$  cluster including the correlation correction (CC) estimated by the three different methods. CC(LSDA) and CC( $X\alpha$ ) denote the calculations with the CC factors estimated from the single-electron calculations using the LSDA potential and the  $X\alpha$  potential, respectively. CC(expt) denotes the calculation with the CC factor estimated from the experimental data. The energy of the ground state ( ${}^4A_2$ ) is set at zero. The peak positions of the observed absorption spectrum of ruby reported by Fairbank *et al.* (Ref. 9) are shown together on the right.

absorption spectra. The calculated multiplet energies of ruby are also listed in Table II. For comparison, our previous results using the  $(\text{CrAl}_7\text{O}_{33})^{42-}$  cluster (FCZ approach) are listed together. The multiplet energies calculated by the  $(\text{CrAl}_7\text{O}_{33})^{42-}$  cluster are slightly higher than those calculated by the  $(\text{CrAl}_{14}\text{O}_{48})^{51-}$  cluster (FCZ approach). The reason for this overestimation is ascribable to the underestimation of the effect of covalency due to insufficient aluminum ions. As we have shown previously,<sup>21</sup> the energy of the quartets are significantly overestimated in the DMC approach compared to those in the FCZ approach, although the degeneracy of each peak is significantly improved, indicating that the configuration interactions are taken into account more appropriately. On the other hand, in the results of the CDC approach, both the absolute energy and the degeneracy are reproduced quite well for the quartets. Therefore the CDC approach is the most effective method among the three approaches adopted in the present work. The energies of the doublets are overestimated in all three approaches, due to the underestimation of the effect of electron correlations.

### B. Estimation of CC factor

In order to estimate the correlation correction (CC) factor,  $c$ , from first principles, the transition energy of the spin-flip from  $(t_{2g} \uparrow)^3$  to  $(t_{2g} \uparrow)^2(t_{2g} \downarrow)^1$ ,  $\Delta E$ , was calculated by a spin-unrestricted single-electron calculation. According to the Slater's transition state method,  $\Delta E$  can be evaluated as the single-electron energy difference,  $\varepsilon_{t\downarrow} - \varepsilon_{t\uparrow}$ , in the  $(t_{2g} \uparrow)^{2.5}(t_{2g} \downarrow)^{0.5}$  configuration.<sup>38</sup> For comparison, the calculation was carried out both for the LSDA potential and the  $X\alpha$  potential. In order to specify the method to estimate the CC factor, these approaches are denoted as CC(LSDA) and CC( $X\alpha$ ). The calculated values of  $\Delta E$  were 1.54 eV (LSDA) and 1.98 eV ( $X\alpha$ ). Using these values, the values of  $c$  were determined by Eq. (2.35). In this case the sum of  $k$  was taken over the four states,  ${}^2T_2$ ,  ${}^2T_1$ ,  ${}^2E$ , and  ${}^4A_2$  ( $Sz = \frac{1}{2}$ ), with the degeneracy of  $g_k = 3, 3, 2$ , and 1, respectively. Since Eq. (2.35) cannot be analytically solved, we repeated the procedure of the calculation of the matrix elements and the diagonalization for gradually changed val-

ues of  $c$ , until we got the value of  $c$  satisfying Eq. (2.35). The calculation of the matrix elements was carried out by the CDC approach. The values of  $c$  obtained by CC(LSDA) and by CC( $X\alpha$ ) are 0.646 and 0.844, respectively.

In order to evaluate the validity of the above estimation, the CC factor was also estimated by fitting to the experimental data. This approach will be denoted as CC(expt). The experimental spin-flip transition energy was evaluated similarly using Eq. (2.34), where experimental values listed in Ref. 9 were used instead of  $E_k^E(c)$ . The estimated spin-flip transition energy  $\Delta E$  was 1.90 eV, which is closer to the value obtained by the  $X\alpha$  potential. On the other hand, the calculation using the LSDA potential significantly underestimates the spin-flip transition energy. In the case of CC(expt), the CC factor was calculated by replacing the right hand side of Eq. (2.35) by  $\Delta E$  estimated above. The obtained value of  $c$  was 0.806, which is also much closer to the value by CC( $X\alpha$ ) than the value by CC(LSDA). This result is probably due to the open shell problem of LDA. It is frequently pointed out that the total energy obtained by LDA underestimates the Coulomb repulsion energy for the open shell systems with fractional occupancy. In such a case, the correction to the Coulomb repulsion energy ( $U$ ) is sometimes introduced (LDA+ $U$  approximation).<sup>39,40</sup> Therefore the underestimation of the spin-flip transition energy in the calculation using the LSDA potential is probably arising from the underestimation of the Coulomb repulsion energy intrinsic to LDA. On the other hand, the  $X\alpha$  potential tends to overestimate the Coulomb repulsion energy for a system with relatively larger spin polarization, since the correlation between the electrons with opposite spins is not taken into account explicitly. Therefore, in the present case, the overestimation due to the  $X\alpha$  potential and the underestimation due to the open shell configuration almost canceled. As a result, a satisfactory estimation of the CC factor was achieved by the calculation using the  $X\alpha$  potential.

### C. Multiplet structure with CC

The calculated multiplet structures of ruby including CC estimated by three different methods, CC(LSDA), CC( $X\alpha$ ),

and CC(expt), are shown in Fig. 6. All calculations were carried out by the CDC approach using the (CrAl<sub>14</sub>O<sub>48</sub>)<sup>51-</sup> cluster. When CC is taken into account, energies of the doublets, <sup>2</sup>E, <sup>2</sup>T<sub>1</sub>, and <sup>2</sup>T<sub>2</sub>, decrease significantly in all cases. As expected from the values of the CC factors, the results of CC(LSDA) significantly underestimate the doublet energies. On the other hand, the results of CC(Xα) and CC(expt) well reproduced the observed values. The difference between the results of CC(Xα) and CC(expt) is relatively small. Therefore, in the present paper, the multiplet structure of ruby will be mainly analyzed based on the results of CC(Xα) and CC(expt). The energies of the quartets, <sup>4</sup>T<sub>2</sub>, <sup>4</sup>T<sub>1a</sub>, and <sup>4</sup>T<sub>1b</sub>, also slightly decrease due to CC, but the changes are much smaller than those of the doublets. Thus the effect of electron correlations is much greater in the doublets. The reason for this is related to the electronic configuration of these states. The quartets <sup>4</sup>T<sub>2</sub>, <sup>4</sup>T<sub>1a</sub>, and <sup>4</sup>T<sub>1b</sub> mainly consist of the (t<sub>2g</sub>)<sup>2</sup>(e<sub>g</sub>)<sup>1</sup>, (t<sub>2g</sub>)<sup>2</sup>(e<sub>g</sub>)<sup>1</sup>, and (t<sub>2g</sub>)<sup>1</sup>(e<sub>g</sub>)<sup>2</sup> configurations, respectively, while the doublets <sup>2</sup>E, <sup>2</sup>T<sub>1</sub>, and <sup>2</sup>T<sub>2</sub> and the ground state all mainly consist of the (t<sub>2g</sub>)<sup>3</sup> configuration. Therefore the energy of these quartets are dominated by the value of the crystal-field split Δ<sub>eff</sub> while the energy of these doublets are dominated by the values of the electron-electron repulsion integrals. Therefore the effect of CC is greater in the doublets in the present case.

The calculated multiplet energies of ruby including the three types of CC are also listed in Table II. In the results of CC(Xα), the peak positions of the observed spectrum are reproduced quite satisfactorily without referring to any experimental data. For comparison, the results of single-electron calculations by Ohnishi and Sugano<sup>10</sup> and Xia *et al.*<sup>11</sup> are listed together. In these calculations, the energies of only the R line and the U band were evaluated since no simple relation was obtained between the energies of other multiplets and the single-electron orbital energies. Our calculation reproduced the R-line energy better than that of Ohnishi *et al.* while their calculation reproduced the U-band energy slightly better than ours. However, considering the fact that they adopted a simple model cluster consisting of seven atoms, in which the ligand oxygen ions are located at regular cubic positions, the good agreement of the U-band energy in their calculation was probably due to the cancellation of the various approximations. As we have already mentioned in Sec. III C, one of the possible reasons for the overestimation of the U-band energy is the effect of the structural relaxation around the impurity chromium ion. It is reported by several authors that the Cr-O bond lengths in ruby are slightly longer than the Al-O bond lengths in α-Al<sub>2</sub>O<sub>3</sub>.<sup>12,41</sup> Thus we roughly estimated the effect of the structural relaxation using a small cluster consisting of seven atoms. Since the structural relaxation mostly occurs in the position of the nearest-neighbor oxygen ions, we calculated the crystal-field split for an unrelaxed (CrO<sub>6</sub>)<sup>9-</sup> cluster and a relaxed (CrO<sub>6</sub>)<sup>9-</sup> cluster. The unrelaxed cluster was constructed based on the crystal data of α-Al<sub>2</sub>O<sub>3</sub>. For the construction of the relaxed cluster, we adopted the results of the pair-potential calculation reported by Kizler *et al.*,<sup>41</sup> which are consistent with the extended x-ray-absorption fine-structure (EXAFS) data reported in the same paper. According to their calculation, the Cr-O bond lengths are slightly extended to 1.91 and 2.00 Å from the original values of 1.86 and 1.97 Å.

TABLE III. Composition of the atomic orbitals within each impurity-state orbital (%) obtained by the (CrAl<sub>14</sub>O<sub>48</sub>)<sup>51-</sup> cluster. O denotes the total of six first-neighbor oxygen ions, and Al denotes the total of 14 aluminum ions.

		t <sub>2g</sub> (a)	t <sub>2g</sub> (e)	e <sub>g</sub> (e)
Cr	3d	90.1	91.3	80.5
	4s	0.1	0.0	0.0
	4p	0.1	0.1	0.6
	total	90.3	91.4	81.1
O	2s	0.2	0.1	1.9
	2p	6.1	4.9	12.4
	total	6.3	5.0	14.3
Al	3s	0.8	1.3	1.3
	3p	0.6	0.9	1.5
	3d	1.6	1.0	1.2
	total	3.0	3.2	4.0

Since the crystal-field split is mostly dominated by the bond lengths, only the bond lengths were changed in the relaxed cluster from the unrelaxed cluster and the direction of the bonds were left unchanged for simplicity. The calculated value of the crystal-field split for the relaxed cluster is smaller than that for the unrelaxed cluster by 0.16 eV. Therefore both the U-band energy and the Y-band energy are expected to decrease roughly by 0.16 eV. Although the complete analysis of the effect of the structural relaxation is beyond the scope of the present paper, if the structural relaxation is taken into account, the agreement with the experiment will be improved.

#### D. Effect of covalency

According to the Mulliken population analysis,<sup>37</sup> the total compositions of the 2s, 2p orbitals of the six first-neighbor O ions are 6.3, 5.0, and 14.3% for the t<sub>2g</sub>(a), t<sub>2g</sub>(e), and e<sub>g</sub>(e) orbitals, respectively, while the total compositions of the 3s, 3p, 3d orbitals of the 14 Al ions are 3.0, 3.2, and 4.0% for the t<sub>2g</sub>(a), t<sub>2g</sub>(e), and e<sub>g</sub>(e) orbitals, respectively as listed in Table III. These results indicate that the degrees of spatial extension of the t<sub>2g</sub> and e<sub>g</sub> states are quite different, although they are assumed to be equal in the traditional ligand-field theory. Such effects were quantitatively analyzed for the TM impurities doped in semiconductors by Watanabe and Kamimura.<sup>20</sup> For example, in the framework of the semiempirical ligand-field theory, the values of two Coulomb integrals J[uv] = ⟨uv|g|uv⟩ and J[uζ] = ⟨uζ|g|uζ⟩ are equal to each other and expressed in terms of the Racah parameters as A - 4B + C,<sup>1</sup> where u and v represent the orbitals of the e<sub>g</sub> symmetry (e symmetry in T<sub>d</sub>) and ζ represents one of the orbitals of the t<sub>2g</sub> symmetry (t<sub>2</sub> symmetry in T<sub>d</sub>). However, they reported that the difference between these integrals is 1.97 eV in the case of Ni<sup>2+</sup> in ZnS and pointed out that to disregard such a large difference could cause a crucial fault in the interpretation of the optical spectra.

For the analysis of the effect of covalency, it is useful to introduce the so-called orbital deformation parameters<sup>18,19</sup> defined by

$$\begin{cases} \lambda_e = J_{\text{MO}}[e_g e_g] / J_{\text{AO}}[e_g e_g] \\ \lambda_t = J_{\text{MO}}[t_{2g} t_{2g}] / J_{\text{AO}}[t_{2g} t_{2g}], \end{cases} \quad (4.1)$$

where  $J_{\text{AO}}$  and  $J_{\text{MO}}$  are the Coulomb integrals calculated by the pure atomic orbitals (AO's) and those calculated by the molecular orbitals (MO's), respectively. Since CC is not included in  $J_{\text{MO}}$ , the effective Coulomb integrals are calculated by multiplying the CC factor  $c$  on the above values of  $J_{\text{MO}}$ ,

$$\begin{cases} J_{\text{eff}}[e_g e_g] = c J_{\text{MO}}[e_g e_g] \\ J_{\text{eff}}[t_{2g} t_{2g}] = c J_{\text{MO}}[t_{2g} t_{2g}]. \end{cases} \quad (4.2)$$

The orbital deformation parameters are often treated as empirical parameters to be determined by fitting to the experimental data. However, in such a semiempirical analysis, the effect of CC is also absorbed in the values of  $\lambda_t$  and  $\lambda_e$ . Therefore the contributions of covalency and that of electron correlations are no longer separable.

In order to evaluate the effect of covalency quantitatively, we have calculated the value of three Coulomb integrals,  $J[e_g(e)e_g(e)]$ ,  $J[t_{2g}(a)t_{2g}(a)]$ , and  $J[t_{2g}(e)t_{2g}(e)]$  from first principles, using the pure AO's and the MO's obtained by the  $(\text{CrAl}_{14}\text{O}_{48})^{51-}$  cluster. The Coulomb integrals for the pure AO's are expressed in terms of the Racah parameters as  $J_{\text{AO}}[e_g(e)e_g(e)] = J_{\text{AO}}[t_{2g}(a)t_{2g}(a)] = J_{\text{AO}}[t_{2g}(e)t_{2g}(e)] = A + 4B + 3C$ . The Racah parameters can be easily calculated from the radial part of the TM-3d AO's,  $R_{3d}(r)$ , using the relation<sup>1</sup>

$$\begin{cases} A = F^0 - \frac{49}{441} F^4 \\ B = \frac{1}{49} F^2 - \frac{5}{441} F^4 \\ C = \frac{36}{441} F^4 \end{cases}, \quad (4.3)$$

where  $F^k$  are Slater integrals defined by

$$F^k = \int_0^\infty r_1^2 dr_1 \int_0^\infty r_2^2 dr_2 R_{3d}^2(r_1) R_{3d}^2(r_2) \frac{r_1^k}{r_2^{k+1}}. \quad (4.4)$$

The calculated values of the Racah parameters<sup>42</sup> are  $A = 20.75$  eV,  $B = 0.13$  eV, and  $C = 0.49$  eV and the Coulomb integrals are calculated as  $J_{\text{AO}}[e_g(e)e_g(e)] = J_{\text{AO}}[t_{2g}(a)t_{2g}(a)] = J_{\text{AO}}[t_{2g}(e)t_{2g}(e)] = 22.74$  eV. These Coulomb integrals are also directly calculated using the MO's of the impurity states obtained by the  $(\text{CrAl}_{14}\text{O}_{48})^{51-}$  cluster. The calculated values are  $J_{\text{MO}}[e_g(e)e_g(e)] = 18.89$  eV,  $J_{\text{MO}}[t_{2g}(a)t_{2g}(a)] = 20.14$  eV, and  $J_{\text{MO}}[t_{2g}(e)t_{2g}(e)] = 20.53$  eV. The values of  $J_{\text{AO}}$  and  $J_{\text{MO}}$  are listed in Table IV. Using these values, the orbital deformation parameters are calculated as,  $\lambda_{e(e)} = 0.831$ ,  $\lambda_{t(a)} = 0.886$ , and  $\lambda_{t(e)} = 0.903$ , as listed in Table V.

### E. Effect of correlation correction

When CC is taken into account,  $J_{\text{MO}}$  are further multiplied by the CC factor  $c$ . As listed in Table V, the value of  $c$  evaluated by CC(expt) and CC( $X\alpha$ ) are 0.806 and 0.844, respectively. For the quantitative analysis of the effect of

TABLE IV. Calculated Coulomb integrals (eV) using the pure Cr-3d atomic orbitals (AO) and molecular orbitals (MO) obtained by the  $(\text{CrAl}_{14}\text{O}_{48})^{51-}$  cluster. CC(expt) and CC( $X\alpha$ ) denote the effective Coulomb integrals calculated by the CC factor estimated from the experimental data and those calculated by the CC factor estimated from the single-electron calculation using the  $X\alpha$  potential, respectively.

	AO	MO	CC(expt)	CC( $X\alpha$ )
$J[e_g(e)e_g(e)]$	22.7	18.9	15.2	16.0
$J[t_{2g}(a)t_{2g}(a)]$	22.7	20.1	16.2	17.0
$J[t_{2g}(e)t_{2g}(e)]$	22.7	20.5	16.6	17.3

CC, the value evaluated by CC(expt) is more appropriate. Thus we first take the value of  $c$  evaluated by CC(expt). Then the effective Coulomb integrals are calculated as  $J_{\text{eff}}[e_g(e)e_g(e)] = 15.2$  eV,  $J_{\text{eff}}[t_{2g}(a)t_{2g}(a)] = 16.2$  eV, and  $J_{\text{eff}}[t_{2g}(e)t_{2g}(e)] = 16.6$  eV, as shown in Table IV. Therefore the Coulomb integrals are significantly reduced due to CC. The effective Coulomb integrals are also calculated using the value of  $c$  evaluated by CC( $X\alpha$ ). The calculated values are  $J_{\text{eff}}[e_g(e)e_g(e)] = 16.0$  eV,  $J_{\text{eff}}[t_{2g}(a)t_{2g}(a)] = 17.0$  eV, and  $J_{\text{eff}}[t_{2g}(e)t_{2g}(e)] = 17.3$  eV, as shown in Table IV. Although the effective Coulomb integrals are slightly overestimated, the difference between the values by CC( $X\alpha$ ) and the values by CC(expt) is quite small. The values of  $c$  indicate that the effect of CC is slightly greater than the effect of covalency and cannot be neglected for the theoretical prediction of the multiplet structure of ruby.

### F. Absorption spectra

Using the explicitly obtained many-electron wave functions, the intensities of the electric-dipole transitions in ruby were calculated by Eq. (2.36). The calculations were carried out by the three different approaches (FCZ, DMC, and CDC) using the  $(\text{CrAl}_{14}\text{O}_{48})^{51-}$  cluster and CC( $X\alpha$ ) was taken into account in all these calculations. If we set the  $C_3$  axis of the cluster parallel to the  $z$  axis, the  $\pi$  spectrum ( $e\parallel C_3$ ) and  $\sigma$  spectrum ( $e\perp C_3$ ) can be expressed by  $I_z$  and  $\frac{1}{2}(I_x + I_y)$ , respectively, where  $I_x$ ,  $I_y$ , and  $I_z$  denote the intensities arising from the electric vector in the direction of  $x$ ,  $y$ , and  $z$  axes, respectively. The contribution of all final states were summed and each state was broadened by a Gaussian function with 0.3 eV full width at half maximum (FWHM) for easy comparison with the experimental data.

The calculated absorption spectra of ruby are shown in Fig. 7 together with the experimental absorption spectra of ruby at 103 K reported by Fairbank *et al.*<sup>9</sup> In the observed

TABLE V. The orbital deformation parameters ( $\lambda$ ) and the correlation correction factors ( $c$ ) calculated using the  $(\text{TMAl}_{14}\text{O}_{48})^{51-}$  cluster (TM=Cr, V).  $c_{\text{expt}}$  and  $c_{X\alpha}$  denote the values estimated from the experimental data and the values estimated from the single-electron calculation using the  $X\alpha$  potential, respectively.

	$\lambda_{e(e)}$	$\lambda_{t(a)}$	$\lambda_{t(e)}$	$c_{\text{expt}}$	$c_{X\alpha}$
$(\text{CrAl}_{14}\text{O}_{48})^{51-}$	0.831	0.886	0.903	0.806	0.844
$(\text{VAl}_{14}\text{O}_{48})^{51-}$	0.829	0.879	0.898	0.704	0.779

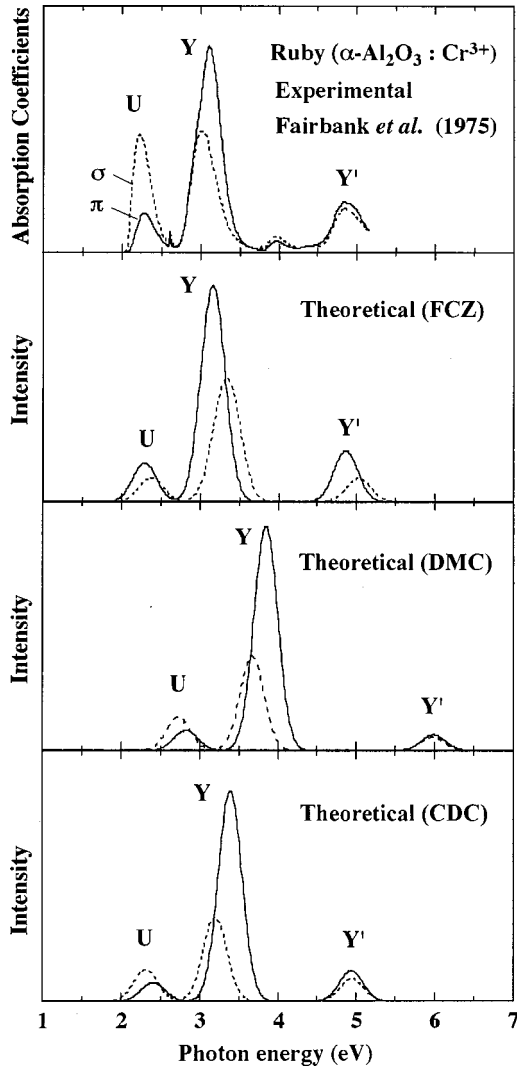


FIG. 7. The intensity of the electric-dipole transition in ruby calculated by the three different approaches (FCZ, DMC, and CDC) using the  $(\text{CrAl}_{14}\text{O}_{48})^{51-}$  cluster, together with the observed absorption spectra of ruby reported by Fairbank *et al.* (Ref. 9). The solid line and the dotted line denote the  $\pi$  spectrum and the  $\sigma$  spectrum, respectively. The  $\pi$  spectrum and the  $\sigma$  spectrum are compared in the same scale. For easy comparison with the observed data, each state is broadened by a Gaussian function with 0.3-eV full width at half maximum (FWHM).

spectra, the intensity of the  $U$  band is greater and the intensity of the  $Y$  band is smaller in the  $\sigma$  spectrum compared to the  $\pi$  spectrum. The peak positions in each peak is slightly different between the  $\pi$  spectrum and the  $\sigma$  spectrum since each  $T$  state splits into  $A$  and  $E$  states due to the trigonal field. In each peak in the  $O_h$  notation, the peak position of the  $\pi$  spectrum shifts toward the higher energy side compared to the corresponding peak in the  $\sigma$  spectrum, indicating that the  $A$  state is above the corresponding  $E$  state. In the observed data, the trigonal splits,  $E_A - E_E$ , for the  $U$  band and the  $Y$  band are 0.05 and 0.10 eV, respectively, and no significant split has been observed for the  $Y'$  band.

In the calculated results of the FCZ approach shown in Fig. 7, the anisotropy of the peak intensities for the  $Y$  band is well reproduced. However, the anisotropy of the peak intensities for the  $U$  band is inconsistent with the experimental

TABLE VI. The trigonal split  $E_A - E_E$  (eV) for each state in the  $O_h$  notation calculated by the three different approaches (FCZ, DMC, and CDC) using the  $(\text{CrAl}_{14}\text{O}_{48})^{51-}$  cluster. For comparison, the experimental trigonal splits estimated from the difference in the peak positions between the  $\pi$  spectrum and the  $\sigma$  spectrum are also listed.

	U	Y	$Y'$
Experimental <sup>a</sup>	0.05	0.1	0.0
FCZ	-0.09	-0.19	-0.17
DMC	0.10	0.18	0.02
CDC	0.09	0.20	0.03

<sup>a</sup>Reference 9.

data. Moreover, contrary to the experimental data, the  $\sigma$  spectrum shifts toward the higher energy side, indicating that the calculated positions of the energy of the  $E$  state is higher than the corresponding  $A$  state. This is also shown in the values of  $E_A - E_E$  listed in Table VI, which are negative in all states. Therefore the FCZ approach provide qualitatively wrong results for the behavior of the trigonal-field splits. On the other hand, in the results of the DMC approach, the relative positions of the  $A$  and  $E$  states are consistent with the experiment. Thus the anisotropy of the peak positions as well as the anisotropy of the peak intensities are well reproduced. The calculated trigonal splits are also shown in Table VI. In spite of such a good reproduction of the trigonal splits, however, the absolute energy of each state is significantly overestimated. This discrepancy is improved in the results of the CDC approach shown in the bottom of Fig. 7. In this case, the absolute energy of each peak is also well reproduced in addition to the anisotropy of the peak positions and the peak intensities. The remaining small discrepancy in the absolute energy is regarded as the effect of the structural relaxation as discussed in Sec. IV C. The calculated trigonal splits are also shown in Table VI. The variation of the splits for each band is in qualitatively good agreement with the observed results.

The calculated oscillator strengths for these transitions are compared with the experimental values reported by Fairbank *et al.*<sup>9</sup> and McClure<sup>43</sup> in Table VII. Although the calculated values are somewhat overestimated, they are still almost in the same order. Therefore the theoretical prediction of the absolute intensity without referring to any experimental data were quite satisfactory. One of the reasons for the remaining small discrepancy is the neglect of the vibrational effect.<sup>6</sup>

TABLE VII. The oscillator strengths of the electric-dipole transition calculated by the CDC approach using the  $(\text{CrAl}_{14}\text{O}_{48})^{51-}$  cluster, together with the experimental values reported by McClure and Fairbank *et al.* (in units of  $10^{-4}$ ).

	$U(\pi)$	$U(\sigma)$	$Y(\pi)$	$Y(\sigma)$	$Y'(\pi)$	$Y'(\sigma)$
Fairbank <i>et al.</i> <sup>a</sup>	0.8	2.6	6	4		
McClure <sup>b</sup>	1.3	4.8	10.2	5.9	1.3	1.2
Theoretical	2.3	3.9	25	10	3.7	2.7

<sup>a</sup>Reference 9.

<sup>b</sup>Reference 43.

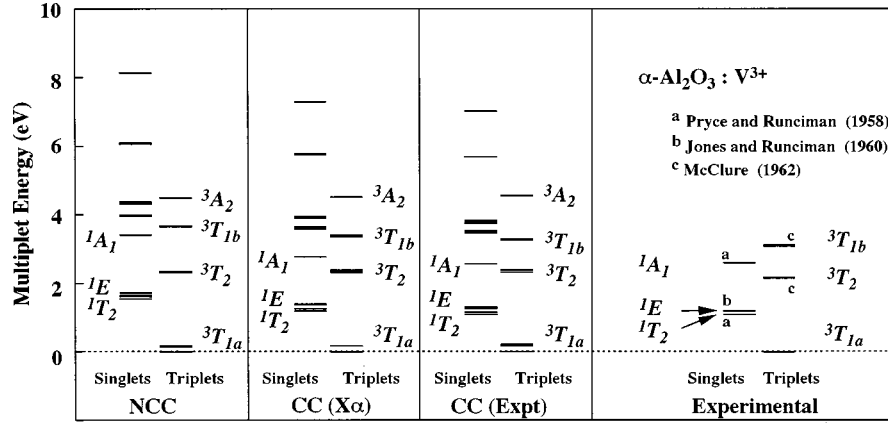


FIG. 8. The multiplet energy levels calculated by the CDC approach using the  $(\text{VA}_{14}\text{O}_{48})^{51-}$  cluster with no correlation correction (NCC) and with correlation correction (CC).  $\text{CC}(X\alpha)$  denotes the calculation with the CC factor estimated from the single-electron calculation using the  $X\alpha$  potential while  $\text{CC}(\text{expt})$  denotes the calculation with the CC factor estimated from the experimental data. Since the ground state  ${}^3T_{1a}$  splits into the A and E states due to the trigonal field, the  ${}^3T_{1a}(A)$  is set at zero. The experimental values reported by several authors (Refs. 43–45) are shown together on the right.

## V. MULTIPLY STRUCTURE OF $\alpha\text{-Al}_2\text{O}_3:\text{V}^{3+}$

### A. Multiplet structure without CC

Since in the analysis of ruby, we found that the CDC approach was the most effective for the theoretical prediction of the multiplet structure, we adopted this approach for the calculation of the multiplet structure of  $\alpha\text{-Al}_2\text{O}_3:\text{V}^{3+}$ . The calculated multiplet structures of  $\alpha\text{-Al}_2\text{O}_3:\text{V}^{3+}$  using the  $(\text{VA}_{14}\text{O}_{48})^{51-}$  cluster with no correlation correction (NCC) is shown on the left in Fig. 8. Since the ground state  ${}^3T_{1a}$  splits into the  ${}^3T_{1a}(A)$  and  ${}^3T_{1a}(E)$  states due to the trigonal field, the energy of the  ${}^3T_{1a}(A)$  state is set at zero. The experimental multiplet energies reported by several authors<sup>43–45</sup> are shown on the right. Since the ground state is a triplet, the transitions to the triplets,  ${}^3T_2$ ,  ${}^3T_{1b}$ , are observed as strong and broad bands, while the transitions to the singlets,  ${}^1T_2$ ,  ${}^1E$ , and  ${}^1A_1$ , are observed as weak and sharp lines. The calculated multiplet energies are listed in Table VIII, together with the experimental values. When CC is not taken into account, the energies of the singlets and the  ${}^3T_{1b}$  state are significantly overestimated while the energy of the  ${}^3T_2$  state is relatively well reproduced.

### B. Estimation of CC factor

The CC factor  $c$  was also evaluated for  $\alpha\text{-Al}_2\text{O}_3:\text{V}^{3+}$ . In this case, the spin-flip from  $(t_{2g}\uparrow)^2$  to  $(t_{2g}\uparrow)^1(t_{2g}\downarrow)^1$ , was considered and the transition energy  $\Delta E$  was evaluated as the single-electron energy difference,  $\varepsilon_{t\downarrow} - \varepsilon_{t\uparrow}$ , in the  $(t_{2g}\uparrow)^{1.5}(t_{2g}\downarrow)^{0.5}$  electronic configuration.<sup>38</sup> For comparison, the calculation was carried out both for the LSDA potential and the  $X\alpha$  potential. The calculated values of  $\Delta E$  were 0.738 eV (LSDA) and 0.963 eV ( $X\alpha$ ). These values were also compared with the value estimated by fitting to the experimental data. Although the observed spectra corresponds to the transition from the  ${}^3T_{1a}(A)$  state, the  $(t_{2g}\uparrow)^2$  configuration corresponds to both the  ${}^3T_{1a}(A)$  and  ${}^3T_{1a}(E)$  states. Therefore the average energy of the  $(t_{2g}\uparrow)^2$  configuration is not zero. The reported value of the energy separation between the  ${}^3T_{1a}(E)$  state and the  ${}^3T_{1a}(A)$  state is 850  $\text{cm}^{-1}$  (Ref. 46) and 960  $\text{cm}^{-1}$ .<sup>43</sup> These values are generally assigned to the components split by the spin-orbit interaction.<sup>13,14</sup> Considering the contribution of the  ${}^3T_{1a}(E)$  state, the average energy of the  $(t_{2g}\uparrow)^2$  configuration ( $\sim 0.07$  eV) should be subtracted from the observed values listed in

TABLE VIII. The multiplet energy levels (eV) calculated by the CDC approach using the  $(\text{VA}_{14}\text{O}_{48})^{51-}$  cluster with no correlation correction (NCC) and with the correlation correction (CC), together with the observed multiplet energies of  $\alpha\text{-Al}_2\text{O}_3:\text{V}^{3+}$  reported by several authors.  $\text{CC}(X\alpha)$  denotes the calculation with the CC factor estimated from the single-electron calculation using the  $X\alpha$  potential while  $\text{CC}(\text{expt})$  denotes the calculation with the CC factor estimated from the experimental data. The calculated multiplet energies are averaged within each state in the  $O_h$  notation.

		${}^1T_2$	${}^1E$	${}^1A_1$	${}^3T_2$	${}^3T_{1b}$
Experimental		1.09 <sup>a</sup>	1.21 <sup>b</sup>	2.61 <sup>a</sup>	2.17 ( $\sigma$ ) <sup>c</sup> 2.16 ( $\pi$ ) <sup>c</sup>	3.09 ( $\sigma$ ) <sup>c</sup> 3.14 ( $\pi$ ) <sup>c</sup>
$(\text{VA}_{14}\text{O}_{48})^{51-}$	NCC	1.61	1.72	3.41	2.33	3.66
$(\text{VA}_{14}\text{O}_{48})^{51-}$	$\text{CC}(X\alpha)$	1.28	1.39	2.78	2.35	3.38
$(\text{VA}_{14}\text{O}_{48})^{51-}$	$\text{CC}(\text{expt})$	1.17	1.28	2.55	2.36	3.28

<sup>a</sup>Pryce and Runciman (Ref. 44).

<sup>b</sup>Jones and Runciman (Ref. 45).

<sup>c</sup>McClure (Ref. 43).

Refs. 43–45 before applying Eq. (2.34). Then the value of  $\Delta E$  was evaluated to be 0.871 eV, which is also closer to the value estimated from the calculation using the  $X\alpha$  potential. Since the calculation by the LSDA potential considerably underestimates the value of  $\Delta E$ , we estimated the CC factor only for CC( $X\alpha$ ) and CC(expt). Using these values of  $\Delta E$ , the value of  $c$  was determined by Eq. (2.35). In this case, the sum of  $k$  was taken over the four states,  $^1T_2$ ,  $^1E$ ,  $^1A_1$ , and  $^3T_{1a}$  ( $S_z=0$ ), with degeneracy of  $g_k=3, 2, 1$ , and 3, respectively. Since the  $^3T_{1a}$  state splits due to the trigonal crystal field, the average energy of the  $^3T_{1a}$  state was taken as the energy of the  $(t_{2g})^2$  configuration. In the case of CC(expt), the right-hand side of Eq. (2.35) is replaced by  $\Delta E$  estimated above. The obtained values of  $c$  were 0.779 and 0.704 for CC( $X\alpha$ ) and CC(expt), respectively. These values are also listed in Table V. In this case, the discrepancy between the value by CC( $X\alpha$ ) and the value by CC(expt) is slightly larger than the case of ruby.

### C. Multiplet structure with CC

When CC is taken into account, the energies of the singlets,  $^1T_2$ ,  $^1E$ , and  $^1A_1$ , significantly decrease as shown in Fig. 8. Although the triplet energies also decrease, the changes are relatively small. Therefore the effect of electron correlations is greater in the singlets than in the triplets. This is also due to the fact that the energies of these singlets are dominated by the electron-electron repulsion integrals, while the energies of these triplets are dominated by the crystal-field split. In the results of the calculation by CC( $X\alpha$ ), the multiplet energies are slightly overestimated. However, the calculated multiplet structure was considerably improved compared to the results without CC. The slight overestimation of the triplet energies are due to the structural relaxation as in the case of ruby.

### D. Effect of covalency

According to the Mulliken population analysis,<sup>37</sup> the total compositions of the  $2s$ ,  $2p$  orbitals of the six first-neighbor O ions are 5.6, 4.3, and 12.0% for the  $t_{2g}(a)$ ,  $t_{2g}(e)$ , and  $e_g(e)$  orbitals, respectively, while the total compositions of the  $3s$ ,  $3p$ ,  $3d$  orbitals of the 14 Al ions are 4.2, 4.3, and 6.1%, for the  $t_{2g}(a)$ ,  $t_{2g}(e)$ , and  $e_g(e)$  orbitals, respectively, as listed in Table IX. As expected from the analysis of the single-electron energy levels, the Al- $3s$ ,  $3p$ ,  $3d$  composition in the impurity states is greater in  $\alpha\text{-Al}_2\text{O}_3:\text{V}^{3+}$  than in ruby, while the O- $2s$ ,  $2p$  composition in the impurity states is smaller in  $\alpha\text{-Al}_2\text{O}_3:\text{V}^{3+}$  than in ruby. On the other hand, the pure TM- $3d$  composition of the impurity states is almost comparable to that in ruby. In order to study the effect of covalency quantitatively, we also calculated the Coulomb integrals,  $J[e_g(e)e_g(e)]$ ,  $J[t_{2g}(a)t_{2g}(a)]$ , and  $J[t_{2g}(e)t_{2g}(e)]$ , using the pure TM- $3d$  AO's and the MO's obtained by the  $(\text{VAl}_{14}\text{O}_{48})^{51-}$  cluster. The Racah parameters calculated using the radial part of the pure V- $3d$  AO's (Ref. 42) are  $A=19.57$  eV,  $B=0.13$  eV, and  $C=0.46$  eV and the Coulomb integrals are calculated as  $J_{\text{AO}}[e_g(e)e_g(e)] = J_{\text{AO}}[t_{2g}(a)t_{2g}(a)] = J_{\text{AO}}[t_{2g}(e)t_{2g}(e)] = A + 4B + 3C = 21.47$  eV. On the other hand, the Coulomb integrals calculated using the MO's of the impurity-state orbitals ob-

TABLE IX. Composition of the atomic orbitals within each impurity-state orbital (%) obtained by the  $(\text{VAl}_{14}\text{O}_{48})^{51-}$  cluster. O denotes the total of six first-neighbor oxygen ions, and Al denotes the total of 14 aluminum ions.

		$t_{2g}(a)$	$t_{2g}(e)$	$e_g(e)$
V	$3d$	89.6	90.9	80.4
	$4s$	0.1		
	$4p$	0.2	0.1	0.7
	total	89.9	91.0	81.1
O	$2s$	0.2	0.1	2.0
	$2p$	5.4	4.2	10.0
	total	5.6	4.3	12.0
Al	$3s$	1.1	1.8	2.6
	$3p$	0.8	1.1	2.0
	$3d$	2.3	1.4	1.5
	total	4.2	4.3	6.1

tained by the  $(\text{VAl}_{14}\text{O}_{48})^{51-}$  cluster are  $J_{\text{MO}}[e_g(e)e_g(e)] = 17.80$  eV,  $J_{\text{MO}}[t_{2g}(a)t_{2g}(a)] = 18.88$  eV, and  $J_{\text{MO}}[t_{2g}(e)t_{2g}(e)] = 19.27$  eV, as listed in Table X. Using these values, the orbital deformation parameters are calculated as,  $\lambda_{e(e)}=0.829$ ,  $\lambda_{t(a)}=0.879$ , and  $\lambda_{t(e)}=0.898$  as listed in Table V. Therefore the effect of covalency is comparable to that in ruby.

### E. Effect of correlation correction

For the quantitative analysis of the effect of CC, the effective Coulomb integrals are calculated using the value of  $c$  estimated by CC(expt). The calculated values are  $J_{\text{eff}}[e_g(e)e_g(e)] = 12.5$  eV,  $J_{\text{eff}}[t_{2g}(a)t_{2g}(a)] = 13.3$  eV, and  $J_{\text{eff}}[t_{2g}(e)t_{2g}(e)] = 13.6$  eV as listed in Table X. Therefore the Coulomb integrals are reduced significantly due to CC. These Coulomb integrals are also calculated using the value of  $c$  estimated by CC( $X\alpha$ ). The calculated values are  $J_{\text{eff}}[e_g(e)e_g(e)] = 13.9$  eV,  $J_{\text{eff}}[t_{2g}(a)t_{2g}(a)] = 14.7$  eV, and  $J_{\text{eff}}[t_{2g}(e)t_{2g}(e)] = 15.0$  eV, as also listed in Table X. Since the value of  $c$  is much smaller than the values of  $\lambda$ , the effect of CC is much greater than the effect of covalency, in this case. Therefore the consideration of CC is quite important for the theoretical prediction of the multiplet structure of  $\alpha\text{-Al}_2\text{O}_3:\text{V}^{3+}$ . The value of  $c$  for  $\alpha\text{-Al}_2\text{O}_3:\text{V}^{3+}$  is slightly smaller than the value obtained for ruby.

TABLE X. Calculated Coulomb integrals (eV) using the pure V- $3d$  atomic orbitals (AO) and molecular orbitals (MO) obtained by the  $(\text{VAl}_{14}\text{O}_{48})^{51-}$  cluster. CC(expt) and CC( $X\alpha$ ) denote the effective Coulomb integrals calculated by the CC factor estimated from the experimental data and those calculated by the CC factor estimated from the single-electron calculation using the  $X\alpha$  potential, respectively.

	AO	MO	CC(expt)	CC( $X\alpha$ )
$J[e_g(e)e_g(e)]$	21.5	17.8	12.5	13.9
$J[t_{2g}(a)t_{2g}(a)]$	21.5	18.9	13.3	14.7
$J[t_{2g}(e)t_{2g}(e)]$	21.5	19.3	13.6	15.0

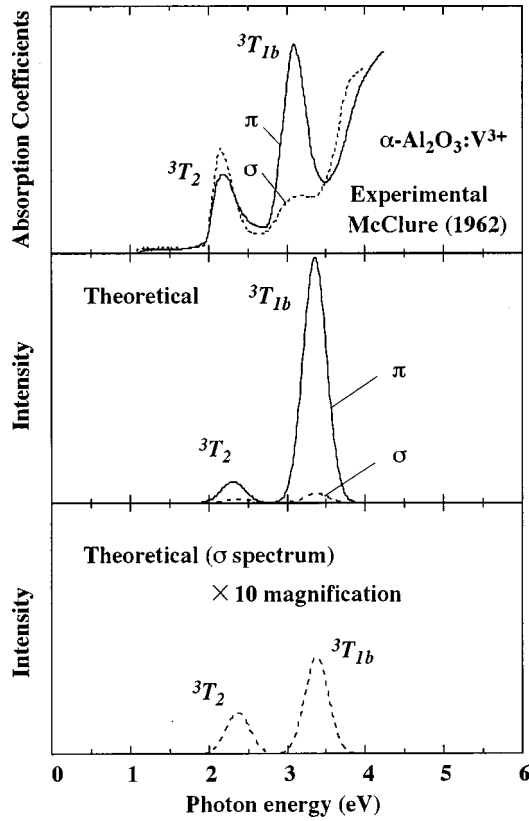


FIG. 9. The intensity of the electric-dipole transition in  $\alpha\text{-Al}_2\text{O}_3:\text{V}^{3+}$  calculated by the CDC approach using the  $(\text{VAI}_{14}\text{O}_{48})^{51-}$  cluster, together with the observed absorption spectrum reported by McClure (Ref. 43). The solid line and the dotted line denote the  $\pi$  spectrum and the  $\sigma$  spectrum, respectively. The  $\pi$  spectrum and the  $\sigma$  spectrum are compared in the same scale. For easy comparison with the observed data, each state is broadened by a Gaussian function with 0.3-eV full width at half maximum (FWHM).

#### F. Absorption spectra

The intensities of the electric-dipole transitions in  $\alpha\text{-Al}_2\text{O}_3:\text{V}^{3+}$  were also calculated by Eq. (2.36). The calculations were carried out by the CDC approach with  $\text{CC}(X\alpha)$  using the  $(\text{VAI}_{14}\text{O}_{48})^{51-}$  cluster (Fig. 9). In this case, the ground state  ${}^3T_{1a}$  splits into the  $A$  and  $E$  states and the energy separation between these states<sup>43,46</sup> ( $\sim 0.11$  eV) is much greater than  $kT$  even in the room temperature, where  $k$  and  $T$  denote the Boltzmann constant and the temperature. Therefore we considered only the transition from the  ${}^3T_{1a}(A)$  state for the calculation of the absorption spectra. Each level was broadened by a Gaussian function with 0.3 eV FWHM for easy comparison with the experimental data.

The calculated results are compared with the absorption spectra of  $\alpha\text{-Al}_2\text{O}_3:\text{V}^{3+}$  at 77 K reported by McClure.<sup>43</sup> In the observed spectra, the intensity for the  ${}^3T_{1b}$  state is much stronger in the  $\pi$  spectrum compared to the  $\sigma$  spectrum, whereas the intensities for the  ${}^3T_2$  state are almost comparable in both spectra. In the  $\sigma$  spectrum, the position of the  ${}^3T_2$  state shift toward the lower energy side, while that of the  ${}^3T_{1b}$  state shift toward the higher energy side compared to the  $\pi$  spectrum.

In the calculated spectra, the transition to the  ${}^3T_{1b}$  state is much stronger in the  $\pi$  spectrum than in the  $\sigma$  spectrum,

TABLE XI. The trigonal split  $E_E - E_A$  (eV) for each state in the  $O_h$  notation calculated by the CDC approach using the  $(\text{VAI}_{14}\text{O}_{48})^{51-}$  cluster. For comparison, the experimental trigonal splits estimated from the difference in the peak positions between the  $\pi$  spectrum and the  $\sigma$  spectrum are also listed.

	${}^3T_{1a}$	${}^3T_2$	${}^3T_{1b}$
Experimental <sup>a</sup>	0.11		0.05
Theoretical	0.19	0.06	0.03

<sup>a</sup>Reference 43.

which is qualitatively consistent with the experimental data, although the intensity ratio of the  $\pi$  spectrum to the  $\sigma$  spectrum for this state is considerably overestimated. On the other hand, the calculated intensity for the  ${}^3T_2$  state is much stronger in the  $\pi$  spectrum than in the  $\sigma$  spectrum, which is opposite to the experimental data. In the calculated results, the peak positions shift toward the higher energy side both for the  ${}^3T_2$  state and for the  ${}^3T_{1b}$  state in the  $\sigma$  spectrum. Therefore both the intensity and the peak position are consistent with the experimental data for the  ${}^3T_{1b}$  state while neither of them are consistent with the experimental data for the  ${}^3T_2$  state. This anomalous polarization has been pointed out by several authors and discussed with relation to the dynamic Jahn-Teller effect in the  ${}^3T_2$  state<sup>47</sup> or in the  ${}^3T_{1a}$  state.<sup>48</sup> However, its origin has not been clearly explained yet. The peaks for the  ${}^3T_2$  state in the  $\pi$  spectrum and the  $\sigma$  spectrum are conventionally assigned to the  ${}^3T_2(E)$  components split by the spin-orbit interaction rather than the  ${}^3T_2(A)$  and  ${}^3T_2(E)$  states,<sup>13,14</sup> however, these assignments are still rather uncertain. Therefore more precise analysis including the spin-orbit interaction and the dynamic Jahn-Teller effect is quite necessary for the complete understanding of the optical spectra of  $\alpha\text{-Al}_2\text{O}_3:\text{V}^{3+}$ .

The calculated trigonal splits for the triplets,  $E_E - E_A$ , are 0.19, 0.06, and 0.03 eV for  ${}^3T_{1a}$ ,  ${}^3T_2$ , and  ${}^3T_{1b}$ , respectively, as shown in Table XI, together with the observed values by McClure.<sup>43</sup> As shown in the table, the behavior of the trigonal splits in the  ${}^3T_{1a}$  and  ${}^3T_{1b}$  states was qualitatively well reproduced. The experimental value of the split in the  ${}^3T_2$  state is not listed since as mentioned above, the assignment of the peaks for the  ${}^3T_2$  state is still ambiguous.

The calculated oscillator strengths are compared with the experimental values obtained by McClure in Table XII. The values for the  $\pi$  spectrum are somewhat overestimated, while the values for the  $\sigma$  spectrum agree well with the experimental values. Although the split of the  ${}^3T_{1a}$  state is relatively large, the transitions from the  ${}^3T_{1a}(E)$  state could influence the absorption spectrum above the temperature comparable to  $\delta/k$  ( $\sim 1300$  K), where  $\delta$  is the trigonal split in the  ${}^3T_{1a}$  state ( $\delta \sim 0.11$  eV). The number of the  $\text{V}^{3+}$  ion in the  ${}^3T_{1a}(A)$  state  $N_A$  and that in the  ${}^3T_{1a}(E)$  state  $N_E$  at finite temperature can be expressed as

$$\begin{cases} N_A(T) = N_t / [1 + 2 \exp(-\delta/kT)] \\ N_E(T) = 2N_t \exp(-\delta/kT) / [1 + 2 \exp(-\delta/kT)], \end{cases} \quad (5.1)$$

where  $N_t$  is the total number of the  $\text{V}^{3+}$  ions [ $N_t = N_A(T) + N_E(T)$ ]. Therefore the temperature dependence of the intensity can be expressed as

TABLE XII. The oscillator strengths of the electric-dipole transition calculated by the CDC approach using the  $(\text{VAI}_{14}\text{O}_{48})^{51-}$  cluster, together with the experimental values reported by McClure (in units of  $10^{-4}$ ). In addition to the transitions from the  ${}^3T_{1a}(A)$  state, the transitions from the  ${}^3T_{1a}(E)$  state were also calculated and listed.

	Initial state	${}^3T_2(\pi)$	${}^3T_2(\sigma)$	${}^3T_{1b}(\pi)$	${}^3T_{1b}(\sigma)$
Experimental <sup>a</sup>	${}^3T_{1a}(A)$	0.27	0.36	5.6	1.6
Theoretical	${}^3T_{1a}(A)$	4.6	0.8	52	2.0
Theoretical	${}^3T_{1a}(E)$	6.9	4.4	14	6.8

<sup>a</sup>Reference 43.

$$\frac{I_i(T)}{I_i(0)} = \frac{1 + 2a \exp(-\delta/kT)}{1 + 2 \exp(-\delta/kT)}, \quad (5.2)$$

where  $a$  is the ratio of the intensity from the  ${}^3T_{1a}(E)$  state to that from the  ${}^3T_{1a}(A)$  state ( $a = I_E/I_A$ ). McClure estimated the value of  $a$  from the observed temperature dependence of the intensity for the  ${}^3T_2$  state and obtained  $a = 6$ . In the results of the present calculation,  $a = (6.9 + 4.4)/(4.6 + 0.8) = 2.1$ . Although the predicted value of  $a$  is somewhat smaller than the experimental value, the increase of intensity at higher temperature could be qualitatively predicted by the first-principles calculation.

## VI. CONCLUSION

The multiplet structures of ruby and  $\alpha\text{-Al}_2\text{O}_3:\text{V}^{3+}$  have been calculated from first principles by a hybrid method of the density-functional theory (DFT) and the configuration interaction (CI) calculation (DFT-CI approach). The impurity-state orbitals were calculated by the spin-restricted density-functional calculation. The many-electron Hamiltonian was diagonalized within the subspace spanned by the Slater determinants constructed from these impurity-state orbitals. For the calculation of the matrix elements, three different approaches were compared. First was a method proposed by Fazzio, Caldas, and Zunger,<sup>18,19</sup> where the single-electron mean-field effects were formally separated from the many-electron effects (FCZ approach). Second was a method, where the matrix elements were calculated directly using the explicit effective Hamiltonian obtained by Watanabe and Kamimura<sup>20</sup> (DMC approach). The third was a combined method of the FCZ approach and the DMC approach, where the configuration-dependent correction (CDC) similar to the FCZ approach was added to the matrix elements of the DMC approach. The characteristics of these approaches were investigated by calculation of the multiplet structure of ruby. In the FCZ approach, the absolute energy of each state was well reproduced but the split of each state due to the trigonal field could not be reproduced even qualitatively due to the octahedral approximation and the neglect of the off-diagonal elements for the matrix elements of the effective single-electron Hamiltonian. In the DMC approach, the trigonal-field splits were consistent with the experimental data but the absolute energies of the quartets were significantly overestimated. In the CDC approach, both the absolute energy and the trigonal splits were well reproduced.

However, the energies of the doublets or singlets could not be reproduced by simple CI calculations. This was due to the underestimation of the effect of electron correlations.

Although the basic multiplet structure can be reproduced by the diagonalization within the subspace spanned by the Slater determinants constructed from the impurity-state orbitals, the number of the Slater determinants in this subspace is not sufficient to describe the electron correlation effects accurately. Therefore in the present work, the correlation correction (CC) factor was introduced to take into account the remaining effect of electron correlations. In the DFT-CI approach, the CC factor can be estimated by the consistency between the spin-unrestricted single-electron DFT calculation and the multiplet calculation. For comparison, the spin-unrestricted DFT calculation was carried out using the LSDA potential proposed by Vosko, Wilk, and Nusair<sup>27,28</sup> and the Slater's  $X\alpha$  potential.<sup>26</sup> In order to evaluate the validity of these estimations, the CC factor was also estimated from the experimental data and compared with the theoretical values. Surprisingly, the value by the  $X\alpha$  potential agrees with the value estimated from the experimental data much better than the value by the LSDA potential. This is probably due to the open-shell problem of LDA. Since in the calculation based on LDA, the electron-electron repulsion energy in the open-shell system with fractional occupancy tend to be underestimated and additional correction to the electron-electron repulsion energy is frequently introduced (LDA +  $U$  approximation<sup>39,40</sup>). On the other hand, the  $X\alpha$  potential tend to overestimate the electron-electron repulsion energy, since the correlation between the electrons with opposite spins is not taken into account explicitly. Therefore in the case of the  $X\alpha$  potential, the overestimation of the electron-electron repulsion due to the  $X\alpha$  potential cancels with the intrinsic underestimation of the electron-electron repulsion in LDA. As a result, the CC factors were estimated well by the calculation using the  $X\alpha$  potential. In fact, the estimation of the CC factor using the  $X\alpha$  potential proved to be quite effective for the theoretical prediction of the multiplet structures in various materials such as  $\text{Be}_3\text{Al}_2(\text{SiO}_3)_6:\text{Cr}^{3+}$  (emerald),<sup>49</sup>  $\text{YAG}:\text{Cr}^{4+}$ ,<sup>50</sup> or  $\text{Mg}_2\text{SiO}_4:\text{Cr}^{4+}$ .<sup>50</sup> However, these good agreements are somewhat accidental and the development of more appropriate methodology for the estimation of the CC factor is quite important.

The effect of covalency and the effect of electron correlations on the multiplet structure were analyzed by evaluating the orbital deformation parameter and the CC factor. For a quantitative analysis, the CC factor estimated from the experimental data was also used as well as the value estimated from the calculation using the  $X\alpha$  potential. In both ruby and  $\alpha\text{-Al}_2\text{O}_3:\text{V}^{3+}$ , the effect of CC was greater than the effect of covalency, indicating that the effect of CC is more important for the theoretical prediction of the multiplet structure.

In the DFT-CI calculation, the many-electron wave functions are obtained explicitly as linear combination of the Slater determinants. Thus we calculated the intensity of the electric-dipole transition arising from the trigonal distortion of the many-electron wave functions. In the case of ruby, the variation of the peak positions and the peak intensities between the  $\pi$  spectrum and the  $\sigma$  spectrum was reproduced quite well from first principles. In the case of  $\alpha\text{-Al}_2\text{O}_3:\text{V}^{3+}$ , the polarization of the  ${}^3T_{1b}$  state could be reproduced quali-

tatively, however, the results for the  ${}^3T_2$  state were inconsistent with the experimental data, probably due to the neglect of the other effects such as the spin-orbit interaction or the dynamic Jahn-Teller effect. The temperature dependence of the intensity for the  ${}^3T_2$  state was predicted by the theoretical intensity ratio of the transitions from the  ${}^3T_{1a}(E)$  state to those from the  ${}^3T_{1a}(A)$  state and the result was qualitatively consistent with the experimental results. However, a more detailed calculation is necessary for the complete understanding of the optical spectra of  $\alpha\text{-Al}_2\text{O}_3\text{:V}^{3+}$ .

The advantages of the DFT-CI calculation compared to the traditional analysis based on the ligand-field theory can be summarized as follows. (1) The multiplet structures of the TM ions in crystals can be predicted without referring to any experimental data. (2) The effect of covalency and the effect of electron correlations can be evaluated quantitatively. (3) The various physical quantities such as the transition prob-

abilities can be calculated directly using the explicitly obtained many-electron wave functions. (4) The electronic structures of many-ion systems can be easily analyzed in the same way.<sup>51</sup>

Among these advantages, the last one is quite important, since many-ion systems cannot be analyzed at all by the traditional ligand-field theory. Such analysis will be quite effective to clarify the ion-ion interactions such as the energy-transfer mechanism within various solid-state laser materials including different impurity ions.

## ACKNOWLEDGMENT

This work was supported by a Grant-in-Aid for Scientific Research from the Ministry of Education, Science, Sports and Culture.

- <sup>1</sup>S. Sugano, Y. Tanabe, and H. Kamimura, *Multiplets of Transition-Metal Ions in Crystals* (Academic, New York, 1970).
- <sup>2</sup>T. H. Maiman, *Nature (London)* **187**, 493 (1960).
- <sup>3</sup>R. A. Forman, G. J. Piermarini, J. D. Barnett, and S. Block, *Science* **176**, 284 (1972).
- <sup>4</sup>J. H. Eggert, K. A. Goettel, and I. F. Silvera, *Phys. Rev. B* **40**, 5724 (1989).
- <sup>5</sup>J. H. Eggert, F. Moshary, W. J. Evans, K. A. Goettel, and I. Silvera, *Phys. Rev. B* **44**, 7202 (1991).
- <sup>6</sup>S. Sugano and Y. Tanabe, *J. Phys. Soc. Jpn.* **13**, 880 (1958).
- <sup>7</sup>S. Sugano and I. Tsujikawa, *J. Phys. Soc. Jpn.* **13**, 899 (1958).
- <sup>8</sup>M. Shinada, S. Sugano, and T. Kushida, *J. Phys. Soc. Jpn.* **21**, 1342 (1966).
- <sup>9</sup>W. M. Fairbank, Jr., G. K. Klauminzer, and A. L. Schawlow, *Phys. Rev. B* **11**, 60 (1975).
- <sup>10</sup>S. Ohnishi and S. Sugano, *Jpn. J. Appl. Phys., Part 2* **21**, L309 (1982).
- <sup>11</sup>S. Xia, C. Guo, L. Lin, and E. E. Ellis, *Phys. Rev. B* **35**, 7671 (1987).
- <sup>12</sup>W. Duan, G. Paiva, Renata M. Wentzcovitch, and A. Fazzio, *Phys. Rev. Lett.* **81**, 3267 (1998).
- <sup>13</sup>H. U. Rahman and W. A. Runciman, *J. Phys. C* **4**, 1576 (1971).
- <sup>14</sup>D. P. Ma, X. D. Ma, J. R. Chen, and Y. Y. Liu, *Phys. Rev. B* **56**, 1780 (1997).
- <sup>15</sup>K. Ogasawara, T. Ishii, Y. Ito, H. Ida, I. Tanaka, and H. Adachi, *Jpn. J. Appl. Phys., Part 1* **37**, 4590 (1998).
- <sup>16</sup>S. Watanabe and H. Kamimura, *J. Phys. Soc. Jpn.* **56**, 1078 (1987).
- <sup>17</sup>S. Watanabe and H. Kamimura, *J. Phys. C* **20**, 4145 (1987).
- <sup>18</sup>A. Fazzio, M. Caldas, and A. Zunger, *Phys. Rev. B* **29**, 5999 (1984).
- <sup>19</sup>A. Fazzio, M. Caldas, and A. Zunger, *Phys. Rev. B* **30**, 3430 (1984).
- <sup>20</sup>S. Watanabe and H. Kamimura, *Mater. Sci. Eng., B* **3**, 313 (1989).
- <sup>21</sup>K. Ogasawara, T. Ishii, I. Tanaka, and H. Adachi, *Mater. Trans., JIM* **40**, 396 (1999).
- <sup>22</sup>J. P. Perdew and Y. Wang, *Phys. Rev. B* **33**, 8800 (1986).
- <sup>23</sup>J. P. Perdew and Y. Wang, *Phys. Rev. B* **40**, 3399 (1989).
- <sup>24</sup>J. P. Perdew and Y. Wang, *Phys. Rev. B* **45**, 13 244 (1992).
- <sup>25</sup>F. M. F. de Groot, *J. Electron Spectrosc. Relat. Phenom.* **67**, 529 (1994).
- <sup>26</sup>J. C. Slater, *Quantum Theory of Molecules and Solids* (McGraw-Hill, New York, 1974), Vol. 4.
- <sup>27</sup>S. H. Vosko and L. Wilk, *Phys. Rev. B* **22**, 3812 (1980).
- <sup>28</sup>S. H. Vosko, L. Wilk, and M. Nusair, *Can. J. Phys.* **58**, 1200 (1980).
- <sup>29</sup>D. E. Ellis and G. S. Painter, *Phys. Rev. B* **2**, 2887 (1970).
- <sup>30</sup>H. Adachi, M. Tsukada, and C. Satoko, *J. Phys. Soc. Jpn.* **45**, 875 (1978).
- <sup>31</sup>I. Tanaka, J. Kawai, and H. Adachi, *Phys. Rev. B* **52**, 11 733 (1995).
- <sup>32</sup>I. Tanaka and Hirohiko Adachi, *Phys. Rev. B* **54**, 4604 (1996).
- <sup>33</sup>I. Tanaka, M. Mizuno, and H. Adachi, *Phys. Rev. B* **56**, 3536 (1997).
- <sup>34</sup>H. Kanda, M. Yoshiya, F. Oba, K. Ogasawara, H. Adachi, and I. Tanaka, *Phys. Rev. B* **58**, 9693 (1998).
- <sup>35</sup>S. R. Nishitani, S. Fujii, M. Mizuno, I. Tanaka, and H. Adachi, *Phys. Rev. B* **58**, 9741 (1998).
- <sup>36</sup>M. Mizuno, I. Tanaka, and H. Adachi, *Phys. Rev. B* **59**, 15 033 (1999).
- <sup>37</sup>R. S. Mulliken, *J. Chem. Phys.* **23**, 1833 (1955).
- <sup>38</sup>Strictly speaking, the  $t_{2g}$  state splits into the  $(t_{2g}:a)$  and  $(t_{2g}:e)$  states and there are some choices for the electronic configuration of the transition state. Although the calculated  $\Delta E$  is quite insensitive to the choice of the configuration, we adopted the  $(t_{2g}:a\uparrow)^{5/6}(t_{2g}:e\uparrow)^{5/6}(t_{2g}:e'\uparrow)^{5/6}(t_{2g}:a\downarrow)^{1/6}(t_{2g}:e\downarrow)^{1/6}(t_{2g}:e'\downarrow)^{1/6}$  configuration for ruby and the  $(t_{2g}:a\uparrow)^{1/2}(t_{2g}:e\uparrow)^{1/2}(t_{2g}:e'\uparrow)^{1/2}(t_{2g}:a\downarrow)^{1/6}(t_{2g}:e\downarrow)^{1/6}(t_{2g}:e'\downarrow)^{1/6}$  configuration for  $\alpha\text{-Al}_2\text{O}_3\text{:V}^{3+}$ , in order to evaluate the average effect, where two degenerate  $e$  states are distinguished by  $e$  and  $e'$ . The value of  $\Delta E$  was obtained as the difference between the average energy of the  $t_{2g}\downarrow$  state and that of the  $t_{2g}\uparrow$  state.
- <sup>39</sup>V. I. Anisimov, I. V. Solovyev, M. A. Korotin, M. T. Czyzyk, and G. A. Sawatzky, *Phys. Rev. B* **48**, 16 929 (1993).
- <sup>40</sup>V. I. Anisimov, F. Aryasetiawan, and A. I. Lichtenstein, *J. Phys.: Condens. Matter* **9**, 767 (1997).
- <sup>41</sup>P. Kizler, J. He, D. R. Clarke, and P. R. Kenway, *J. Am. Chem. Soc.* **79**, 3 (1996).

- <sup>42</sup>In the present work, the Racah parameters are calculated using the numerically obtained AO's during the single-electron calculation of the (TMA<sub>14</sub>O<sub>48</sub>)<sup>51-</sup> cluster (TM=Cr, V). The effective charges of Cr and V estimated by the Mulliken's method are +2.19 and +2.32, respectively, in the unit of the charge of an electron. The numerical AO's are generated under the potential produced by these effective charges.
- <sup>43</sup>D. S. McClure, *J. Chem. Phys.* **36**, 2757 (1962).
- <sup>44</sup>M. H. L. Pryce and W. A. Runciman, *Discuss. Faraday Soc.* **26**, 34 (1958).
- <sup>45</sup>G. D. Jones and W. A. Runciman, *Proc. Phys. Soc. London* **76**, 996 (1960).
- <sup>46</sup>S. Foner and W. Low, *Phys. Rev.* **120**, 1585 (1960).
- <sup>47</sup>W. C. Scott and M. D. Sturge, *Phys. Rev.* **146**, 262 (1966).
- <sup>48</sup>M. Abou-Ghantous, C. A. Bates, and L. C. Goodfellow, *J. Phys. Chem. Solids* **37**, 1059 (1976).
- <sup>49</sup>T. Ishii, K. Ogasawara, I. Tanaka, and H. Adachi, *Adv. Quant. Chem.* (to be published).
- <sup>50</sup>T. Ishii, K. Ogasawara, I. Tanaka, and H. Adachi (unpublished).
- <sup>51</sup>T. Ishii, K. Ogasawara, I. Tanaka, and H. Adachi, *Mater. Trans., JIM* **40**, 416 (1999).